High viscosity and two phases observed over a range of relative humidities in biomass burning organic aerosol from Canadian wildfires

Nealan G. A. Gerrebos,[1] Julia Zaks,[1] Florence K. A. Gregson,[1] Max Walton-Raaby,[2†] Harrison Meeres,[3‡] Ieva Zigg,[3] Wesley F. Zandberg,[3] Allan K. Bertram[1]*

Author affiliations:
[1] Department of Chemistry, University of British Columbia, Vancouver, British Columbia V6T 1Z1, Canada
[2] Department of Chemistry, Thompson Rivers University, Kamloops, British Columbia V2C 0C8, Canada
[3] Department of Chemistry, University of British Columbia-Okanagan, Kelowna, British Columbia V1V 1V7, Canada
* bertram@chem.ubc.ca

Abstract

Biomass burning organic aerosol (BBOA) is a major contributor to organic aerosol in the atmosphere. The impacts of BBOA on climate and health depend strongly on their physicochemical properties, including viscosity and phase behaviour (number and types of phases); these properties are not yet fully characterized. We collected BBOA field samples during the 2021 British Columbia wildfire season to constrain the viscosity and phase behaviour at a range of relative humidities, and compared them to previous studies on BBOA. Particles from all samples exhibited two-phased behaviour with a polar hydrophilic phase and a non-polar hydrophobic phase. We used the poke-flow viscosity technique to estimate the viscosity of the particles. Both phases of the BBOA had viscosities $>10^8$ Pa s at relative humidities up to 50%. Such high viscosities correspond to mixing times within 200 nm BBOA particles of >5 h. Two phases and high viscosity have implications for how BBOA should be treated in atmospheric models.

Keywords

Biomass burning, organic aerosol, viscosity, phase behaviour, phase separation

Synopsis

This study examines the viscosity and phase behaviour of biomass burning organic aerosol (BBOA) collected from wildfires in Western Canada. The field-collected BBOA contains two organic phases and is highly viscous, with implications for modelling studies of BBOA.

Introduction

Aerosols, small liquid or solid particles suspended in the air, are found throughout the troposphere and originate from both anthropogenic (e.g. vehicle exhaust) and natural sources (e.g. wildfires). Biomass burning is a significant contributor to aerosol concentrations in most regions of the

https://doi.org/10.26434/chemrxiv-2024-5p8pn-v2 **ORCID:** https://orcid.org/0000-0002-5621-2323 Content not peer-reviewed by ChemRxiv. **License:** CC BY 4.0

world.[1–8] Smoke from biomass burning consists of mostly organic aerosol, referred to as biomass-burning organic aerosol (BBOA).[9] For example, smoke sampled from wildfires in the western U.S.A. consisted of > 90% BBOA.[10,11] BBOA can cause negative health effects.[1,12–15] In addition, BBOA contains light absorbing molecules known as brown carbon (BrC) that warm the climate by absorbing sunlight.[16–20] BBOA also acts as nuclei for liquid cloud droplets and possibly ice clouds, thereby indirectly modifying the climate.[21–23] As climate change continues, the frequency and intensity of wildfires is increasing in many regions due to rising temperatures and changing precipitation patterns.[24–27] This should cause the portion of aerosols attributed to biomass burning to grow.

Viscosity and phase behavior (number and types of phases) influence the role of BBOA in air quality and climate. For example, if BBOA contains two phases, then the equilibrium partitioning of gas phase species into the BBOA is changed compared to the non-phase separated case, which impacts how the particles grow and gain mass – in turn influencing their health and climate impacts.[28–30] The presence of two non-crystalline phases has also been shown to change cloud condensation nuclei activity.[31–33] Compared to a well-mixed droplet, a phase-separated droplet with a low polarity organic outer phase has lower surface tension, which lowers the barrier to cloud condensation.[33] If the BBOA particles are sufficiently viscous, the viscosity could limit reactions within the particles by limiting intra-particle diffusion rates.[34–41] Furthermore, if BBOA particles have a viscosity > 10^{12} Pa s (i.e. the particles are in a glassy state), they may be good nuclei for crystalline ice and influence the properties and frequency of ice clouds.[22]

Several studies have directly or indirectly determined the viscosity of laboratory-generated BBOA using the poke-flow technique, volatility measurements, and fluorescence techniques.[34,35,42,43] Several studies have also investigated the phase behavior of laboratory-generated BBOA using optical, fluorescence, and electron microscopy techniques.[34,44–49] While the previous laboratory studies have been useful, the composition of BBOA in the real atmosphere may be different than the composition of BBOA generated in the laboratory for several reasons including atmospheric aging of BBOA, higher degrees of dilution, and burning conditions (e.g. fuel type, temperature, humidity, availability of oxygen). These factors could lead to atmospheric BBOA having a very different viscosity than what is assumed based on laboratory results, and phase behaviour may differ as well.[50,51] Particularly, phase separation has been explained as being driven by differences in polarity, approximated by the oxygen-to-carbon ratio (O:C).[52–57] Atmospheric aging increases O:C,[58,59] so atmospheric aging of particles could change their phase behaviour.

Field studies of the viscosity and phase behavior of BBOA have relied mostly on electron microscopy measurements. In these studies, a type of BBOA known as tar balls has been identified alongside other organic particles.[60–63] Tar balls are operationally defined as particles that are spherical and stable when viewed with an electron microscope. The fact that they are still spherical after collection on an electron microscope substrate indicates that the viscosity of tar balls is very high ($\gtrsim 10^9$ Pa s) at the conditions used for collection.[64] Most often electron microscopy measurements are carried out under a vacuum. Hence, a limitation of electron microscopy analysis of BBOA is that high volatility organic aerosol is likely lost in these studies.[65,66]

https://doi.org/10.26434/chemrxiv-2024-5p8pn-v2 **ORCID:** https://orcid.org/0000-0002-5621-2323 Content not peer-reviewed by ChemRxiv. **License:** CC BY 4.0

In the following, we carried out complementary studies to those described above, aiming to improve our understanding of the phase behavior and viscosity of BBOA. We investigated the viscosity and phase-behavior of BBOA samples collected from forest fire smoke in British Columbia, Canada. Viscosity was probed with the poke-flow technique and phase-behavior was measured with optical microscopy as a function of relative humidity (RH). All experiments were carried out at atmospheric pressure.

Methods and Materials

BBOA Collection. Forest fire BBOA was collected on 47 mm PTFE membrane filters (MTL, USA) at the University of British Columbia – Okanagan (Kelowna, Canada) and Thompson Rivers University (Kamloops, Canada) (see sample locations in Figure S1) in early August 2021 during heavy forest fire activity. Here we focus on two samples: one collected in Kelowna from August 3rd to August 6th and one collected in Kamloops from August 2nd to August 5th. $PM_{2.5}$ concentrations during the two sampling periods reached over 200 µg m^{-3}, according to British Columbia air quality monitoring stations located in the same cities as the collection sites (Figure S2). The air quality monitoring stations were approximately 10 km away in Kamloops and 2 km away in Kelowna. Data was acquired from the BC Air Data Archive Website.[67] $PM_{2.5}$ concentrations during sampling were on average higher in Kamloops than in Kelowna (Figure S2, Table S1). From January 1st 2021 to June 20th 2021, before the start of the wildfire season, the mean daily $PM_{2.5}$ concentrations in Kelowna and Kamloops were 4.8 and 5.5 µg m^{-3}, respectively (Figure S3, Table S1).

Satellite measurements show many forest fires surrounding Kamloops and Kelowna during sampling (Figure S1). Fire locations were gathered from the Fire Information for Resource Management System (FIRMS) U.S./Canada, using data from VIIRS NOAA-20, VIIRS S-NPP, MODIS Aqua and MODIS Terra.[68]

Forests in the burnt regions primarily consist of trees in the *Pinaceae* family, such as Douglas-fir and lodgepole pine.[69,70] Back trajectories suggest that the field samples contained smoke from fires of varying distance from the collection sites and had an atmospheric age of approximately 12 hours or less (Figure S1). The back trajectories were run with the HYSPLIT transport and dispersion model on the READY website from NOAA Air Resources Laboratory (ARL).[71,72] Back trajectories were run once every 12 hours during the sampling period with a starting height of 0 m and using GFS meteorology (0.25 degrees, global).

For sampling, scroll pumps (Agilent, USA) were used to draw approximately 30 L min^{-1} through the filters until roughly 5 mg of $PM_{2.5}$ was collected on each filter. The mass on each filter was estimated based on $PM_{2.5}$ concentrations from the air quality monitoring stations located in the same cities as the collection sites (Figure S2) and daily in-line flow meter measurements (Mass Flow Meter 4043, TSI, USA). Based on calculations using archived hourly air quality data, we estimate that the Kelowna sample had 4.5 mg of $PM_{2.5}$, 88% of which was from wildfires, while the Kamloops sample had 8.1 mg of $PM_{2.5}$, 96% from wildfires (Table S1).

Sample Preparation. BBOA filters were extracted with a 1/1 (v/v) solution of methanol (HPLC grade, Sigma-Aldrich)/water (HPLC grade, Thermo Scientific). Filters were cut into quarters and

https://doi.org/10.26434/chemrxiv-2024-5p8pn-v2 **ORCID:** https://orcid.org/0000-0002-5621-2323 Content not peer-reviewed by ChemRxiv. **License:** CC BY 4.0

placed in glass vials into which 1.5 mL of solvent was added, and then shaken on a platform shaker at 200 rpm for 2 hours. Afterwards, the solutions were passed through 13 mm diameter, 0.45 μm pore Fluoropore membrane syringe filters (Millipore, USA) to remove soot and other insoluble components. Filtered extracts were stored in glass vials at 4°C and wrapped in aluminum foil to limit their exposure to light and avoid any photochemistry. Hems et al. and Trofimova et al. showed that water extracts 70-75% of unaged BBOA, while organic solvents, including methanol, are able to extract nearly 100% of unaged BBOA mass.[73,74] As BBOA is aged, the amount that can be extracted with water is expected to increase and the amount extracted with methanol may decrease as oxidation will increase BBOA's polarity. We therefore expect our extract to have recovered between 70 to 100% of the organic aerosol material from the filters.

Phase behaviour. Samples for phase behaviour experiments were prepared by nebulizing extracts of the BBOA filters onto 13 mm diameter glass slides coated with FluoroPel 800 (Cytonix, USA), a hydrophobic coating, to promote spherical droplet formation. Extracts were nebulized using a syringe pump and a pneumatic nebulizer (Part #G1946-67098, Agilent, USA) with a sheath gas flow of 15 L min^{-1} to dry the particles (Figure S4). The particles were then collected on the glass slides using a micro-orifice uniform deposit impactor (MOUDI-II 120, TSI, USA) (Figure S4). After impaction, the slides were conditioned at 95% relative humidity (RH) overnight above a saturated KNO_3 solution in a sealed jar.[75] The high RH values allowed for the impacted particles to take up water and grow and take on more spherical shapes, which are better for imaging. To observe the phase behaviour, the slides were imaged at relative humidity values ranging from 0-100% within an RH-controlled flow cell with glass windows coupled to a microscope (Axiotech 100 HD reflected-light microscope, Zeiss, Germany).[76] The RH was ramped from 0 to 100% over the course of 2 hours, then decreased back to 0% RH over 2 hours. Results are only shown for decreasing RH experiments since the same behavior was observed when the RH was increased and decreased.

Poke-flow measurements. The poke-flow technique was used to constrain the viscosities of the inner and outer phases of the BBOA particles.[77–79] Poke flow measurements were done on the same prepared samples used for the phase behaviour measurements. The setup was similar to that used previously.[78–81] The samples were put in a humidified flow cell which has a window on the bottom to allow viewing by an inverted microscope (ME1400TC-INF, AmScope, USA). The cell also has a hole in the top, sealed by a flexible latex membrane, through which an ultrafine needle (13561-10, Ted Pella Inc., USA) is inserted. The needle is moved using a micromanipulator to poke BBOA particles. Experiments were conducted at 30%, 40%, 50%, and 60% RH, and the particles were conditioned in the flow cell for 3 hours before being poked. Poking caused the particles to crack if they were highly viscous, or else resulted in the formation of a hole in the particle which would recover over time to reduce the surface free energy of the system. Images of the particles were recorded for 2 hours after poking. Each measurement was taken at least twice.

At 30%, 40%, and 50% RH, the particles cracked and did not flow during the 2 hour observation time (see below). For these cases, the viscosity is assigned $\gtrsim 2.5\times10^8$ Pa s based on fluid dynamics simulations in COMSOL Multiphysics 5.4 (COMSOL, Sweden) with a quarter sphere model of a cracked particle.[78,80,81] In short, the viscosity in the simulation was adjusted until the edge of the cracked particles in the simulation moved by 0.5 μm in 2 hours. In the simulations we assumed

https://doi.org/10.26434/chemrxiv-2024-5p8pn-v2 **ORCID:** https://orcid.org/0000-0002-5621-2323 Content not peer-reviewed by ChemRxiv. **License:** CC BY 4.0

that the surface tension was 30 mN m^{-1} and the slip length was 5 nm, as conservative lower limits. The viscosity that gave 0.5 μm of movement in 2 hours was 2.5×10^8 Pa s. Since the movement in our experiments was less than 0.5 μm (based on the resolution of our microscope), and the surface tension and slip length used in the simulations were conservative lower limits, a viscosity of 2.5×10^8 should be consider a lower limit to the viscosities in the experiments when cracking and no flow was observed over 2 hours.

At 60% RH, the particles did not crack and rather a hole formed and slowly recovered over time (see below). Fluid dynamics simulations based on a half-torus model have been developed to determine the viscosity of single-phase particles that formed a hole after poking and slowly recovered.[78,79] However, in the current experiments, the BBOA particles contain two phases (see below). Since the previously developed half-torus model is based on single-phase particles, we did not attempt to apply this model to the current results. Developing and testing a half-torus model for two-phase particles is beyond the scope of the current study. Along with designing a new model, we would need information about the interactions between the two phases, e.g. the interfacial tension, which is not information we have knowledge of. As a result, we were not able to assign a viscosity to the poke flow experiments at 60% RH. Our approach of only assigning a viscosity to multiphase particles that cracked and did not flow is similar to the approach used by others when constraining the viscosity of field-collected multiphase samples.[82,83]

Samples for the poke-flow experiments were prepared by nebulizing 1/1 (v/v) solutions of methanol and water containing BBOA extracts. Even though the BBOA particles were exposed to a methanol-free carrier gas for an extended time after formation, we cannot rule out trace amounts of residual methanol remaining in the BBOA particles from the extraction process. For RH values of 0-50 %, we report a lower limit to the viscosity of the field-collected BBOA samples based on the observations that the particles shatter and did not flow (see below). The further removal of any residual methanol from the BBOA particles would not change the reported lower limits to viscosity, since methanol has a low viscosity and removal of any residual methanol would only increase the viscosity of our particles.

Aerosol Mass Spectrometry. A high-resolution time-of-flight Aerosol Mass Spectrometer (HR-ToF-AMS) (Aerodyne, USA) was used to measure the mass spectra of the BBOA extracts. The working principle and operation of the HR-ToF-AMS are described in detail elsewhere;[84–86] briefly, the AMS measures electron-ionization mass spectra of aerosol particles sampled from ambient air and can report the bulk aerosol quantities of organics, nitrate, sulfate, ammonium, and chloride mass concentrations. The vaporizer current was set to 1 A. To prepare the sample in a form that could be sampled by the AMS, extracts were nebulized using the same syringe pump pneumatic nebulizer used for the phase behaviour measurements (Figure S4). After nebulization, samples were diluted and dried with a sheath gas flow of 10 to 15 L min^{-1}. The aerosol then passed through a home-built diffusion dryer packed with 30 cm of molecular sieves (Type 4A beads 8-12 mesh, Supelco, Germany) and 30 cm of activated charcoal (Sigma-Aldrich, USA) to remove any residual water and methanol, respectively, and then sampled by the AMS (Figure S4). High-resolution AMS data were processed using Squirrel v1.66 and PIKA 1.26 in the Igor Pro software environment (WaveMetrics, USA). Elemental ratios were estimated using the Improved Ambient

https://doi.org/10.26434/chemrxiv-2024-5p8pn-v2 **ORCID:** https://orcid.org/0000-0002-5621-2323 Content not peer-reviewed by ChemRxiv. **License:** CC BY 4.0

method[87] using peaks up to m/z 180, since over 93% of the mass was contained in m/z below 180 for all samples. For each sample, we report the mean oxygen-to-carbon ratio (O:C), hydrogen-to-carbon ratio (H:C), and carbon oxidation state ($\overline{OS}_C \approx 2 \times O{:}\,C - H{:}\,C$).[88]

Results and Discussion

Chemical composition of the BBOA particles. The AMS results (Figure S5 and Table 1) indicate that both the BBOA samples were mainly organic (> 90 wt %), which is consistent with previous measurements of BBOA from laboratory burns of pine wood.[11] The O:C was 0.73-0.74, which is higher than for freshly emitted laboratory BBOA and unaged field BBOA but consistent with some BBOA aged for intermediate timescales.[2,89]

Table 1. Composition and oxidation state of BBOA samples obtained from AMS analysis.

Sample	Mass fraction					Mean oxidation		
	Organic	NO_3	NH_4	SO_4	Cl	O:C	H:C	$\overline{OS}_c$
Kamloops	0.93	0.032	0.026	0.0075	0.0055	0.73 ± 0.20[a]	1.45 ± 0.19[b]	0.02 ± 0.5[c]
Kelowna	0.94	0.024	0.035	0.0041	0.0023	0.74 ± 0.21[a]	1.45 ± 0.19[b]	0.04 ± 0.5[c]

[a,b] The uncertainties for O:C and H:C ratios are 28% and 13%, respectively, based on the results for standards reported by Canagaratna et al. for the improved ambient method.[87]

[c] The ± 0.5 uncertainty associated with $\overline{OS}c$ is also from the improved ambient method.[87]

Phase behavior. Both samples showed two phases across the full range of RH values (Figure 1). Phase behaviour results were the same when increasing and decreasing the RH. Others have shown that phase separation can occur in mixtures of primary organic aerosol (POA) and secondary organic aerosol (SOA), and in mixtures of different types of SOA, if the organic molecules making up the mixtures have a difference of > 0.2 in O:C values.[52,53,56,57] In addition, previous studies have shown that unaged BBOA can contain organic molecules with a wide range of O:C values.[2,90] Therefore, phase separation in our BBOA can be explained by a large difference in O:C values of the organic molecules making up the BBOA. Our samples also likely contain secondary BBOA in addition to primary BBOA. Secondary BBOA should have organic molecules with higher O:C values than primary BBOA,[58,59] further enhancing phase separation when mixed with primary BBOA. Phase separation in aerosol particles can also be driven by the coexistence of organic and inorganic salts which are soluble in water,[44,91,92] but the AMS results (Table 1) indicate that BBOA samples from both sites were mainly organic. Hence, the presence of inorganic salts was most likely not the main driver for the two phases.

https://doi.org/10.26434/chemrxiv-2024-5p8pn-v2 **ORCID:** https://orcid.org/0000-0002-5621-2323 Content not peer-reviewed by ChemRxiv. **License:** CC BY 4.0

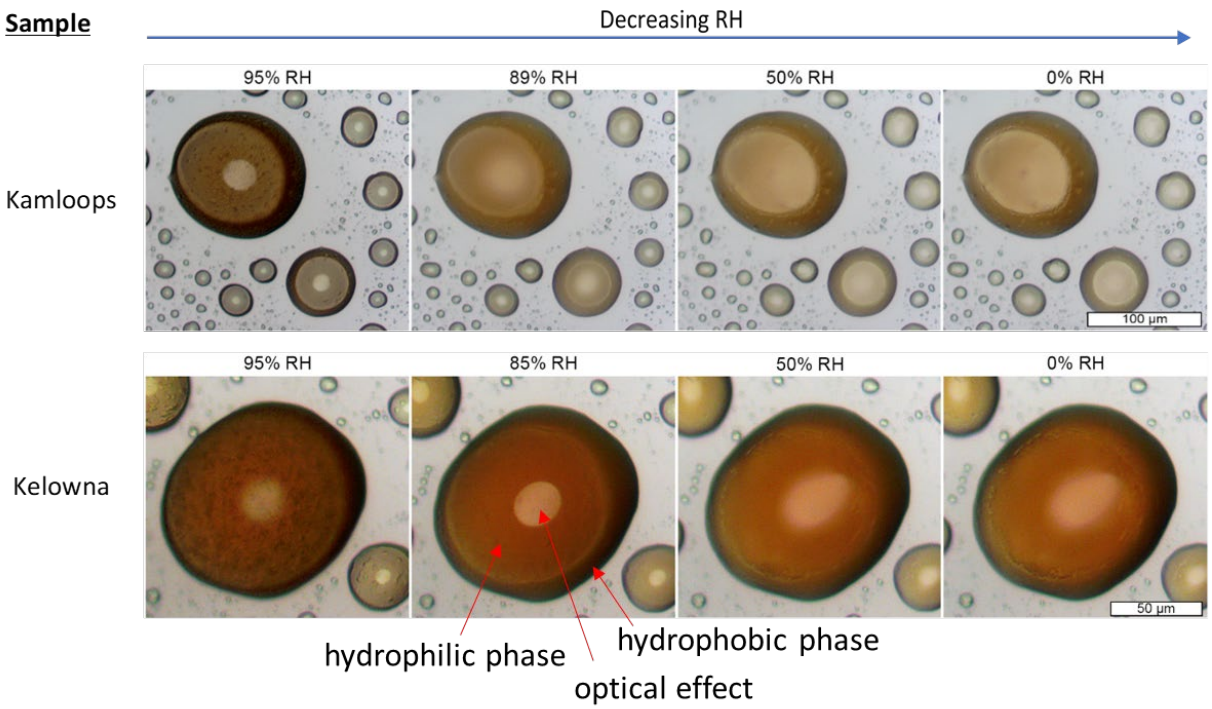

Figure 1. Images from the Kamloops sample (top) and Kelowna sample (bottom) extracts, showing two phases, as the RH was decreased from ~95% to 0%. The images and RH values in the figure were selected to show a representative range of the BBOA's phase behavior. The small white ellipses in the centers of many of the droplets are reflections/optical effects from the microscope's lamp.

It is likely that very low polarity compounds in the BBOA samples, such as long-chain hydrocarbons, were not extracted by methanol and water. If these compounds are present in the whole BBOA prior to sampling, they should have an even lower O:C than any compounds we extracted, thereby increasing the tendency for there to be phase separation.

In most cases, the particles assumed an approximately core-shell morphology. The outer phase can be identified as a less polar, hydrophobic organic phase while the inner phase is the more polar and hydrophilic of the two. As humidity increased in the flow cell, the inner phase usually swelled, showing that it was more hydrophilic and more polar. Higher polarity is generally expected to lead to higher surface tension, thus the higher polarity compounds are expected to comprise the inner phase to minimize the total surface energy of the system, assuming enough time for diffusion and equilibration within the particles.[93] Others have shown that methanol-soluble BrC from biomass burning has a higher absorption of light than water-soluble BrC, suggesting that most of the colour comes from the less polar molecules.[94] We should therefore expect the low-polarity hydrophobic outer phase to be darker in colour, which is indeed observed in the particles in Figure 1.

Viscosity. The viscosities of the BBOA were probed using the poke-flow technique. If the particles cracked upon being poked and then did not show any signs of recovery after 2 hours, they were classified as being amorphous solids (also known as glassy) or highly viscous semi-solids with viscosities of at least 2.5×10^{8} Pa s.[78,80,81] Amorphous solids have a viscosity of $>10^{12}$ Pa s and

https://doi.org/10.26434/chemrxiv-2024-5p8pn-v2 **ORCID:** https://orcid.org/0000-0002-5621-2323 Content not peer-reviewed by ChemRxiv. **License:** CC BY 4.0

semi-solids have a viscosity between 10^2 and 10^{12} Pa s.[95] For details, see the Methods and Materials section.

As shown in Figure 2, both the Kamloops and the Kelowna samples shattered at 30% RH and the shards did not show any signs of flowing. Experiments were not conducted at drier conditions, because lowering the RH can only lead to the same or even higher viscosities, and therefore the same shattering result.[64] At 40% RH, the particles also shattered with no signs of flow. For the Kamloops sample, the poke in the center of the droplet did not cause cracks to extend all the way to the outer phase, so another poke was made in the outer phase as quickly as possible (near the top of the particle in Figure 2, second row), and this poke caused clear cracks in the outer phase.

At 50% RH, poking the center of the Kamloops sample caused cracks in the outer phase but only a hole in the inner phase, without cracks. For the Kelowna sample at the same relative humidity, a poke in the center caused cracks from the center to the outer edge. Again, there were no signs of recovery in any of the cracked particles at 40 or 50% RH. We conclude that our samples had at least one phase that was semi-solid or amorphous solid with a viscosity $\geq 2.5\times10^8$ Pa s for RH values of 50% or less. The bottom panel in Figure 3 shows the distributions of hourly RH measurements in Kamloops and Kelowna. The RH at both Kamloops and Kelowna during sample collection was often below 50%. Hence, RH values of 50% or less are often relevant for our samples.

	Kamloops			Kelowna		
RH (%)	Before poking	Immediately after poking	2 hours	Before poking	Immediately after poking	2 hours
30	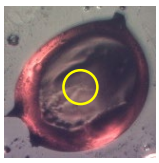	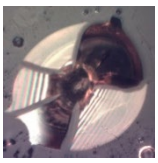		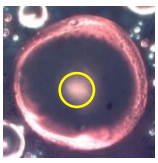	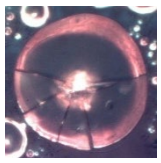	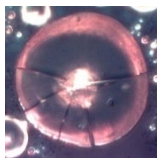
40	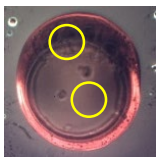	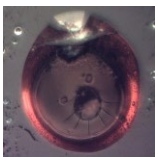	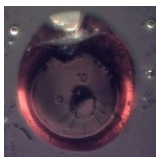		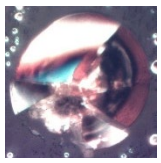	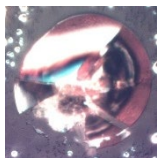
50	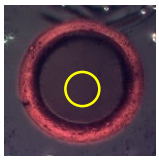	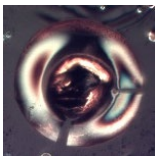	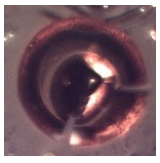	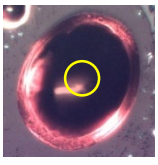	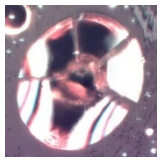	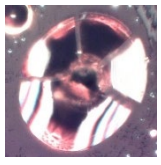
60	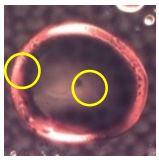	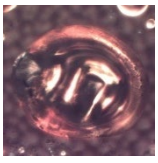	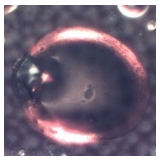	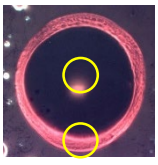	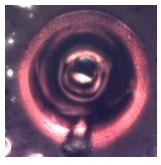	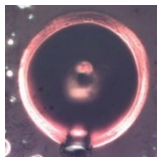

https://doi.org/10.26434/chemrxiv-2024-5p8pn-v2 **ORCID:** https://orcid.org/0000-0002-5621-2323 Content not peer-reviewed by ChemRxiv. **License:** CC BY 4.0

Figure 2: Poke-flow results for the BBOA extracts at select RH values. Images were captured before the particles were poked, immediately after being poked, and then 2 hours after being poked. Yellow circles in the pre-poke images indicate where the particles were poked. The coloration of the droplets here looks different from those in Figure 1 because the microscope and the humidity-controlled cell are different, leading to different lighting.

At 60% RH, both samples were poked once in the inner phase and once on the outer phase (Figure 2, fourth row), forming holes in the particles with no signs of cracking. After 2 hours, the hole in the middle almost fully recovered while the outer phase did not move. The unmoving outer phase may have been due to a difference in the total restorative forces acting on the outer edge of the droplet compared to the middle and the thinness of the outer phase, or, alternatively, the outer phase may have been more viscous than the inner phase. Without fluid dynamics simulations that include the geometry and interfacial tensions of the two phases, it is not possible to conclusively distinguish between these cases. Experiments were not conducted at > 60% RH, because a higher RH can only lead to lower viscosities as the particles take up water.[64]

The Kelowna and Kamloops samples comprised 88% and 96% wildfire BBOA, respectively (Table S1). We estimated the influence of background non-BBOA on our measured viscosities using calculations based on the Arrhenius-type mixing rule (Supplementary Information Section S1).[96] The calculations show that the background non-BBOA does not have a large influence on the lower limits to viscosities reported here for the BBOA. E.g. the presence of background non-BBOA could, at most, decrease our reported lower limit by a factor of 3 for the Kelowna sample.

Comparison with previous BBOA phase behavior measurements. The observation of two phases is consistent with the results by Gregson et al. who observed two phases in BBOA particles generated from smoldering pine wood in the laboratory and sampling BBOA directly on microscope slides using an impactor and without extraction with a solvent.[34] Visual differences between our samples in Figure 1 herein and Figure 1 in Gregson et al. are likely, in large part, due to the different types of microscopes being used (fluorescence in Gregson et al. vs. optical herein). The fact that the impacted BBOA in Gregson et al. shows the same phase behaviour as our extracts possibly suggests that a mixture of methanol and water extracted a wide enough range of the compounds in BBOA to accurately describe its phase behaviour.

Jahn et al. also observed that some particles from the combustion of sawgrass in the laboratory displayed two organic phases under dry conditions (0% RH) using electron microscopy. Two distinct organic phases have also been observed in field-collected BBOA samples under dry conditions. China et al. observed two distinct types of tar balls in field samples, one less oxidized than the other.[47] Hand et al. and Tivanski et al. also found that some types of tar balls in field-collected samples had more oxygen in the outer layers.[48,49] The later observations are consistent with two phases, although the observations of a more hydrophilic phase on the outside of the particles are opposite to our observations. Nevertheless, we do not know if tar balls were present in our field samples and if tar balls are extracted well by our solvent system (methanol-water). Related, Hand et al. observed that some types of tar balls take up water above 75 % RH.[48] In

https://doi.org/10.26434/chemrxiv-2024-5p8pn-v2 **ORCID:** https://orcid.org/0000-0002-5621-2323 Content not peer-reviewed by ChemRxiv. **License:** CC BY 4.0

contrast, Semeniuk et al., Adachi and Buseck, and Dusek et al. showed that some types of tar balls are hydrophobic or only weakly hygroscopic.[63,97,98] Overall, our results provide additional evidence that field-collected BBOA can contain two phases. Moreover, our results illustrate that the two phases can persist over a wide range of relative humidity values (~95 to 0 % RH).

Comparison with previous BBOA viscosity measurements. As shown in Figure 3, our BBOA field samples have higher viscosities under more humid conditions than several other BBOA samples generated in the laboratory.[34,35,42,43] Kiland et al. used poke-flow to measure the viscosity of SOA made from the oxidation of BBOA-like phenolic compounds, as a proxy for biomass burning SOA. Those samples were highly viscous and cracked at low RH, but their viscosities decreased by an order of magnitude at 20% RH.[42] Schnitzler et al. used poke-flow to measure the viscosity of water-soluble extracts of primary BBOA generated in the lab from smoldering pine wood. The water-soluble BBOA consistently had a viscosity lower than Kiland et al.'s SOA, and far lower than the field samples herein.[35]

Gregson et al. used the fluorescence recovery after photobleaching (FRAP) method to measure the diffusion coefficients of fluorescent dyes in BBOA and then converted the results into the viscosity of the hydrophobic phase and the hydrophilic phase of the BBOA. Gregson et al. reported viscosities of about 10^2 Pa s at 30% RH and 293 K for both phases, estimated from the diffusion coefficients measurements.[34] This is far lower than our field BBOA.

Xu et al. reported the glass transition temperature and viscosity of unaged and aged BBOA generated from the combustion of pine wood, poplar wood, cedar wood and cornstalk using flaming conditions.[43] Glass transition temperatures and viscosities were calculated from volatility measurements, which assumes that the BBOA particles contained a single phase. At 35% RH and 298.15 K, the viscosities of those unaged samples ranged from 9.95×10^4 to 4.22×10^5 Pa s. After aging using an OH exposure equivalent to 1.5 days in the atmosphere, the viscosities of the BBOA from wood fuels increase by factors of 2.5 to 13. The viscosity of BBOA from burnt cornstalk was halved after the same aging time. Nevertheless, even after aging, the viscosity of the laboratory-generated BBOA was orders of magnitude less viscous than our field BBOA samples at 30-40% RH.

The higher viscosities of our field samples are most likely due to a combination of factors. It could be partially explained by oxidation, which is expected to lead to more polar compounds, higher intermolecular forces, and therefore higher viscosities in the BBOA.[90,99,100] However, Xu et al.'s experiments show that on timescales relevant to our study, oxidation alone could not bring the viscosity of BBOA to 2.5×10^8 Pa s. Such high viscosities could also be due to dilution in the atmosphere prior to sampling. When smoke plumes are diluted, low molecular weight and low polarity compounds can evaporate first, leaving behind larger, more polar, and hence more viscous compounds.[90,101] Recent experiments by Siemens et al. suggest that this dilution can cause an increase in the viscosity of BBOA by up to 3 orders of magnitude.[102] The differences in viscosities could also be due to differences in burn conditions (i.e. flaming vs smoldering) or fuel type. Most of the studies above burn a single wood or fuel type at a single temperature, while our field samples contained BBOA from fires that would have been burning at different temperatures and a wide

https://doi.org/10.26434/chemrxiv-2024-5p8pn-v2 **ORCID:** https://orcid.org/0000-0002-5621-2323 Content not peer-reviewed by ChemRxiv. **License:** CC BY 4.0

range of fuels could have contributed to the samples. Additional studies are needed to explore the effect of atmospheric oxidation, dilution, and burning conditions on BBOA viscosity.

In addition to the studies above, tar balls have been observed in a few laboratory studies using electron microscopy.[98,103,104] Tar balls have also been observed often in field-collected samples of biomass burning smoke using electron microscopy. Studies show their number fractions increase during the first 5 hours of aging but decrease at longer times.[62,66,105] As discussed above, we do not know if tar balls were present in our field samples and if tar balls are extracted well by our solvent system (methanol-water). If tar balls were not extracted well by our solvent system, then our results indicate the existence of a type of highly viscous non-tar ball BBOA.

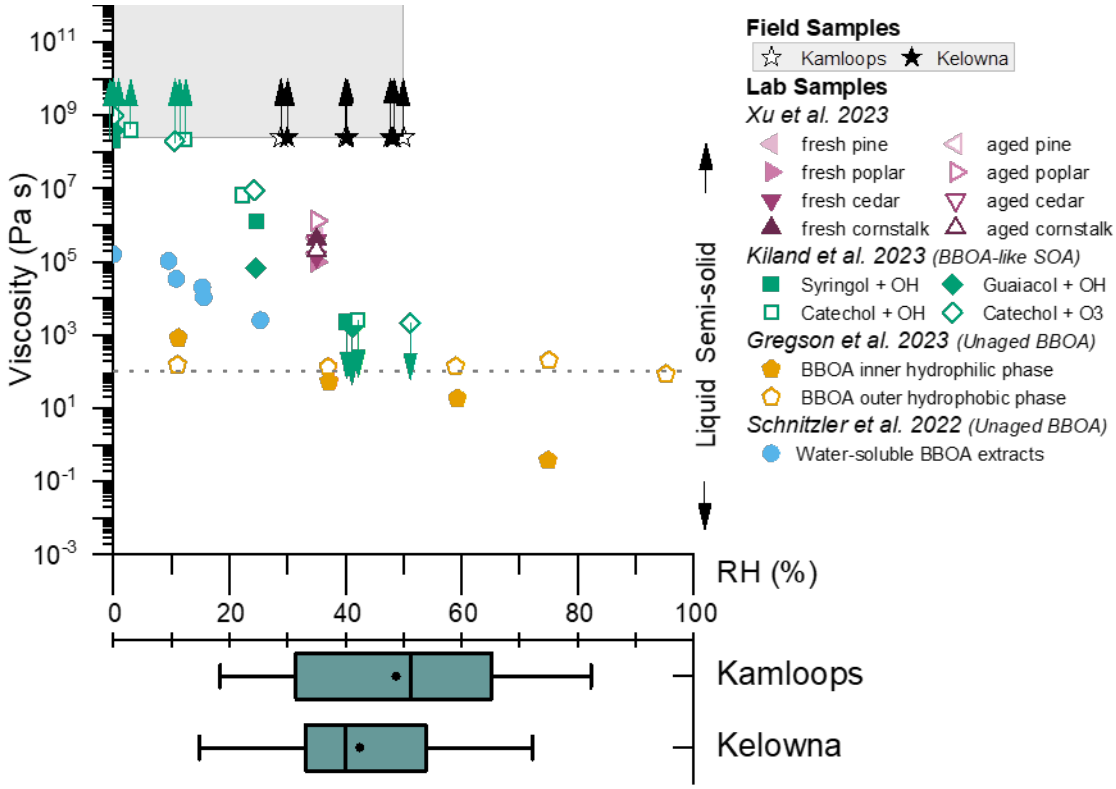

Figure 3. Previously measured viscosities of lab-generated primary BBOA (Schnitzler et al. 2022, Xu et al. 2023, and Gregson et al. 2023), oxidation flow reactor-aged BBOA (Xu et al. 2023), and oxidatively aged secondary BBOA proxies (Kiland et al. 2023) compared to the viscosities observed for the Kamloops and Kelowna BBOA samples.[42,35,34] Upward and downward arrows on data points indicate that viscosities are a minimum or maximum value, respectively, for the viscosity of the aerosol under those conditions. The grey shaded region represents the possible range of field sample BBOA viscosities. The poke-flow experiments show the viscosity is ≥ 2.5×10^{8} Pa s from 30-50%. Viscosities are also ≥ 2.5×10^{8} Pa s at 0 to 30 % RH, since viscosity only increases as the RH decreases. Box plots in the bottom panel show the distributions of hourly RH measurements in Kamloops and Kelowna, with black dots showing the mean RH, the boxes showing the median and 25th and 75th percentiles, and the whiskers showing the minimum and maximum values.

https://doi.org/10.26434/chemrxiv-2024-5p8pn-v2 **ORCID:** https://orcid.org/0000-0002-5621-2323 Content not peer-reviewed by ChemRxiv. **License:** CC BY 4.0

Implications

Most atmospheric models that treat biomass burning organic aerosols, and organic aerosols in general, consider them as single-phased particles for gas-particle partitioning calculations.[35,106–108] In addition, some models have treated primary organic aerosols and secondary organic aerosols as two separate phases.[109,110]

The results herein show that BBOA, at least in regions where forests primarily consist of pine trees, should be treated as having two separate phases. Depending on the degree of internal/external mixing of BBOA in forest fire plumes, these two phases may coexist and be separated within individual particles. This is without considering the mixing state of soot/black carbon (BC) with BBOA in wildfire plumes, which can also have different degrees of internal and external mixing and depends on the age of the plume.[17,111,112] BC may be coated with a layer of BBOA, so if the BBOA is phase-separated, it is possible to have BC cores engulfed in 2 distinct layers of BBOA. In addition, BC in two-phased particles can preferentially partition into the lowest polarity phase depending on coating thickness, which may modify the absorption of sunlight by BC.[113,114]

Phase separation in aerosols impacts the partitioning of species between the gas and particle phase. If BBOA contain a single phase, then semivolatile organic compounds can partition into the entire aerosol mass. On the other hand, if phase separation occurs, semivolatile organic compounds may only partition into a portion of the aerosol mass, reducing the gas-to-particle partitioning of semivolatile organic compounds. Therefore, models that assume single-phase BBOA may be overestimating particle growth.[55,115–119] Phase separation within individual particles can increase the cloud condensation nucleation activity of organic aerosols by moving the lower surface tension organics to the outside of the particle.[32,92]

To account for two phases in BBOA, atmospheric models could assume two phases and model SVOCs partitioning only into the more polar phase. In addition, atmospheric models could assume that the low polarity phase does not take up water, while the high polarity phase takes up water with a given hygroscopicity. If phase separation occurs within individual particles, the outer low polarity phase could form a complete or partial surface active organic monolayer, which enhances cloud condensation nucleation activation, similar to the approaches in Ovadnevaite et al. and Ruehl et al.[33,120] Experiments are needed to test these speculations.

We found that both phases of Kamloops and Kelowna BBOA samples had viscosities $\geq 2.5\times10^{8}$ Pa s at relative humidities up to 50%. Based on a fractional Stokes-Einstein equation, a 200 nm diameter BBOA particle would have a mixing time of ≥5.7 hours if the viscosity is $\geq 2.5\times10^{8}$ Pa s (Supplementary Information S3).[121]

In Schnitzler et al. and Gregson et al., the viscosity of lab-generated BBOA was used to estimate the lifetime of BrC due to ozonolysis.[34,35] As BrC reacts with ozone, it can be "bleached" and lose its absorptive properties, changing its impact on the climate.[35,122] This process is slowed down when BBOA/BrC is highly viscous, as it takes longer for ozone to diffuse into the aerosol. The experiments here predict that BBOA in the field will be more viscous than reported by Schnitzler et al. and Gregson et al. at RH values of 50% and below (Figure 3).[34,35] Under conditions where fresh lab-generated BBOA would be a liquid, the field sample BBOA would be a solid, and the

https://doi.org/10.26434/chemrxiv-2024-5p8pn-v2 **ORCID:** https://orcid.org/0000-0002-5621-2323 Content not peer-reviewed by ChemRxiv. **License:** CC BY 4.0

lifetimes of processes like ozonolysis would be even longer than predicted in Schnitzler et al. and in Gregson et al. This framework can be extended and applied to other reactions in BBOA that have diffusion-limited kinetics.

Biomass burning events emit large amounts of primary BBOA and precursors of secondary BBOA. After emission, the primary BBOA can partially evaporate and secondary BBOA can form on and in the primary BBOA.[58,107] A highly viscous BBOA, as observed here, could limit the rate of evaporation of primary BBOA and the formation rate of secondary BBOA.[123–128] A recent modelling study that investigated the evolution of BBOA by evaporation of primary BBOA and the formation of secondary BBOA assumed the BBOA was liquid-like with a diffusion coefficient of 10^{-10} m^2 s^{-1}.[107] Additional modelling studies are needed to determine the effect of highly viscous BBOA on the evolution of BBOA in the atmosphere and the resulting impact on predicted BBOA mass and composition.

The high viscosity may also have an impact on ice-cloud nucleation. Some studies have suggested that glassy organic aerosol can act as heterogeneous nuclei for ice clouds.[22,129–133] The forest fire BBOA in this study was only highly viscous up to 50% RH at room temperature, but viscosity also increases as temperatures get colder. Hence, the RH threshold at which cracking occurs will be extended to higher RH values at higher, colder altitudes. In the upper troposphere, where temperatures and RH values are often low,[134] BBOA might often be in an amorphous solid (i.e. glassy) state. Consistent with this speculation, previous studies have observed ice nucleation in smoke plumes in the free troposphere.[135] However, the nucleation of ice by glassy organic aerosol is still an active area of debate with a recent study suggesting that ice nucleation by glassy organic aerosol may be less important than previously suggested.[136] Studies that focus on ice nucleation by glassy BBOA are needed to resolve the importance of glassy BBOA for ice cloud formation in the upper troposphere.

A caveat to the implications above is that the particles used in our work were 60 to 120 μm in diameter, which is at least several times larger than atmospheric particles (approximately 10 nm to 10 μm in diameter). Finite size effects can suppress liquid-liquid phase separation when the diameter is $\lesssim$ 40 nm.[137] In addition, finite size effects may sharply decrease viscosities of organic aerosols when the diameter is $\lesssim$ 100 nm.[138] Thus, we anticipate that our results apply to particles larger than approximately 100 nm, which covers most of the mass of BBOA in the atmosphere,[139–141] but experiments are needed to verify this hypothesis.

The viscosity of our field samples was much higher than that of some previously measured lab-generated BBOA and BBOA proxies.[34,35,42] Therefore, any BBOA studies using lab-generated aerosols as proxies for wildfire BBOA should be mindful of these differences. It is, however, useful to be able to make samples in the lab rather than collecting them in the field as it enables more extensive studies of BBOA behaviour. Experiments as a function of aging, dilution, combustion conditions, and fuel types should be done to bridge the gap between lab and field BBOA and to develop methods for creating more realistic BBOA in the laboratory environment.

https://doi.org/10.26434/chemrxiv-2024-5p8pn-v2 **ORCID:** https://orcid.org/0000-0002-5621-2323 Content not peer-reviewed by ChemRxiv. **License:** CC BY 4.0

Supporting Information

Additional discussion and figures: calculation of the impact of non-BBOA background aerosol, calculation of the mixing time in highly viscous BBOA, maps showing the locations of satellite-detected forest fires and calculated air back-trajectories during field sampling, air quality station data, a schematic of the experimental setup, and aerosol mass spectra (DOCX).

Acknowledgements

We acknowledge the support of the Natural Sciences and Engineering Research Council of Canada (NSERC), [funding reference number RGPIN-2023-05333]. Cette recherche a été financée par le Conseil de recherches en sciences naturelles et en génie du Canada (CRSNG), [numéro de référence RGPIN-2023-05333]. We also acknowledge the support of NSERC for a postgraduate scholarship award [PGS D-579464-2023] for funding N.G.A.G., Mitacs Accelerate and Supra Research and Development for funding I. Z., and NSERC Discovery Grant [RGPIN-2016-03929] and the UBCO Work-Study Program for funding H. M.

We thank UBC Vancouver and UBC Okanagan for the support of a UBC Collaborative Research Mobility Award. We thank Dr. Nelaine Mora-Diez for helping coordinate the measurements at Thompson Rivers University.

We acknowledge the NOAA Air Resources Laboratory (ARL) for the provision of the HYSPLIT transport and dispersion model and READY website (https://www.ready.noaa.gov) used in this publication. We also acknowledge the use of data and imagery from NASA's Fire Information for Resource Management System (FIRMS) (https://earthdata.nasa.gov/firms), part of NASA's Earth Observing System Data and Information System (EOSDIS). We acknowledge the free and open source QGIS software, which was used to combine the HYSPLIT and FIRMS data into maps.

We thank Shantanu Jathar for helpful discussions regarding the impact of high viscosities on the evolution of BBOA in the atmosphere.

This work was conducted on the unceded, traditional, ancestral territories of the Musqueam Nation, the Syilx Okanagan Nation, and the Tk'emlúps te Secwépemc.

Present addresses:

[†]M. W.-R.: University of Waterloo, 200 University Ave W, Waterloo, ON N2L 3G1, Canada
[‡]H. M.: TRIUMF, 4004 Wesbrook Mall, Vancouver, BC V6T 2A3, Canada

References

(1) Chen, J.; Li, C.; Ristovski, Z.; Milic, A.; Gu, Y.; Islam, M. S.; Wang, S.; Hao, J.; Zhang, H.; He, C.; Guo, H.; Fu, H.; Miljevic, B.; Morawska, L.; Thai, P.; Lam, Y. F.; Pereira, G.; Ding, A.; Huang, X.; Dumka, U. C. A Review of Biomass Burning: Emissions and Impacts on Air Quality, Health and Climate in China. *Sci. Total Environ.* **2017**, *579* (November 2016), 1000–1034. https://doi.org/10.1016/j.scitotenv.2016.11.025.

https://doi.org/10.26434/chemrxiv-2024-5p8pn-v2 **ORCID:** https://orcid.org/0000-0002-5621-2323 Content not peer-reviewed by ChemRxiv. **License:** CC BY 4.0

(2) Zhou, S.; Collier, S.; Jaffe, D. A.; Briggs, N. L.; Hee, J.; Sedlacek III, A. J.; Kleinman, L.; Onasch, T. B.; Zhang, Q. Regional Influence of Wildfires on Aerosol Chemistry in the Western US and Insights into Atmospheric Aging of Biomass Burning Organic Aerosol. *Atmospheric Chem. Phys.* **2017**, *17* (3), 2477–2493. https://doi.org/10.5194/acp-17-2477-2017.

(3) Li, H.; Zhang, Q.; Jiang, W.; Collier, S.; Sun, Y.; Zhang, Q.; He, K. Characteristics and Sources of Water-Soluble Organic Aerosol in a Heavily Polluted Environment in Northern China. *Sci. Total Environ.* **2021**, *758*, 143970. https://doi.org/10.1016/j.scitotenv.2020.143970.

(4) Bozzetti, C.; Sosedova, Y.; Xiao, M.; Daellenbach, K. R.; Ulevicius, V.; Dudoitis, V.; Mordas, G.; Byčenkienė, S.; Plauškaitė, K.; Vlachou, A.; Golly, B.; Chazeau, B.; Besombes, J.-L.; Baltensperger, U.; Jaffrezo, J.-L.; Slowik, J. G.; El Haddad, I.; Prévôt, A. S. H. Argon Offline-AMS Source Apportionment of Organic Aerosol over Yearly Cycles for an Urban, Rural, and Marine Site in Northern Europe. *Atmospheric Chem. Phys.* **2017**, *17* (1), 117–141. https://doi.org/10.5194/acp-17-117-2017.

(5) Johnson, M. S.; Strawbridge, K.; Knowland, K. E.; Keller, C.; Travis, M. Long-Range Transport of Siberian Biomass Burning Emissions to North America during FIREX-AQ. *Atmos. Environ.* **2021**, *252* (October 2020), 118241–118241. https://doi.org/10.1016/j.atmosenv.2021.118241.

(6) Wu, Y.; Nehrir, A. R.; Ren, X.; Dickerson, R. R.; Huang, J.; Stratton, P. R.; Gronoff, G.; Kooi, S. A.; Collins, J. E.; Berkoff, T. A.; Lei, L.; Gross, B.; Moshary, F. Synergistic Aircraft and Ground Observations of Transported Wildfire Smoke and Its Impact on Air Quality in New York City during the Summer 2018 LISTOS Campaign. *Sci. Total Environ.* **2021**, *773*, 145030–145030. https://doi.org/10.1016/j.scitotenv.2021.145030.

(7) Carter, T. S.; Heald, C. L.; Cappa, C. D.; Kroll, J. H.; Campos, T. L.; Coe, H.; Cotterell, M. I.; Davies, N. W.; Farmer, D. K.; Fox, C.; Garofalo, L. A.; Hu, L.; Langridge, J. M.; Levin, E. J. T.; Murphy, S. M.; Pokhrel, R. P.; Shen, Y.; Szpek, K.; Taylor, J. W.; Wu, H. Investigating Carbonaceous Aerosol and Its Absorption Properties From Fires in the Western United States (WE-CAN) and Southern Africa (ORACLES and CLARIFY). *J. Geophys. Res. Atmospheres* **2021**, *126* (15), 1–28. https://doi.org/10.1029/2021jd034984.

(8) Schill, G. P.; Froyd, K. D.; Bian, H.; Kupc, A.; Williamson, C.; Brock, C. A.; Ray, E.; Hornbrook, R. S.; Hills, A. J.; Apel, E. C.; Chin, M.; Colarco, P. R.; Murphy, D. M. Widespread Biomass Burning Smoke throughout the Remote Troposphere. *Nat. Geosci.* **2020**, *13* (6), 422–427. https://doi.org/10.1038/s41561-020-0586-1.

(9) Reid, J. S.; Eck, T. F.; Christopher, S. A.; Koppman, R.; Dubovik, O.; Eleuterio, D. P.; Holben, B. N.; Reid, E. A.; Zhang, J. A Review of Biomass Burning Emissions Part II: Intensive Physical Properties of Biomass Burning Particles. *Atmospheric Chem. Phys.* **2005**, *5*, 799–825. https://doi.org/10.5194/acp-5-799-2005.

(10) Liu, X.; Huey, L. G.; Yokelson, R. J.; Selimovic, V.; Simpson, I. J.; Müller, M.; Jimenez, J. L.; Campuzano-Jost, P.; Beyersdorf, A. J.; Blake, D. R.; Butterfield, Z.; Choi, Y.; Crounse, J. D.; Day, D. A.; Diskin, G. S.; Dubey, M. K.; Fortner, E.; Hanisco, T. F.; Hu, W.; King, L. E.; Kleinman, L.; Meinardi, S.; Mikoviny, T.; Onasch, T. B.; Palm, B. B.; Peischl, J.; Pollack, I. B.; Ryerson, T. B.; Sachse, G. W.; Sedlacek, A. J.; Shilling, J. E.; Springston, S.; St. Clair, J. M.; Tanner, D. J.; Teng, A. P.; Wennberg, P. O.; Wisthaler, A.; Wolfe, G. M. Airborne Measurements of Western U.S. Wildfire Emissions: Comparison with Prescribed

https://doi.org/10.26434/chemrxiv-2024-5p8pn-v2 **ORCID:** https://orcid.org/0000-0002-5621-2323 Content not peer-reviewed by ChemRxiv. **License:** CC BY 4.0

Burning and Air Quality Implications. *J. Geophys. Res. Atmospheres* **2017**, *122* (11), 6108–6129. https://doi.org/10.1002/2016jd026315.
(11) May, A. A.; McMeeking, G. R.; Lee, T.; Taylor, J. W.; Craven, J. S.; Burling, I.; Sullivan, A. P.; Akagi, S.; Collett, J. L.; Flynn, M.; Coe, H.; Urbanski, S. P.; Seinfeld, J. H.; Yokelson, R. J.; Kreidenweis, S. M. Aerosol Emissions from Prescribed Fires in the United States: A Synthesis of Laboratory and Aircraft Measurements. *J. Geophys. Res. Atmospheres* **2014**, *119* (20), 11,826-11,849. https://doi.org/10.1002/2014jd021848.
(12) Kim, Y. H.; Warren, S. H.; Krantz, Q. T.; King, C.; Jaskot, R.; Preston, W. T.; George, B. J.; Hays, M. D.; Landis, M. S.; Higuchi, M.; Demarini, D. M.; Gilmour, M. I. Mutagenicity and Lung Toxicity of Smoldering vs. Flaming Emissions from Various Biomass Fuels: Implications for Health Effects from Wildland Fires. *Environ. Health Perspect.* **2018**, *126* (1). https://doi.org/10.1289/EHP2200.
(13) Korsiak, J.; Pinault, L.; Christidis, T.; Burnett, R. T.; Abrahamowicz, M.; Weichenthal, S. Long-Term Exposure to Wildfires and Cancer Incidence in Canada: A Population-Based Observational Cohort Study. *Lancet Planet. Health* **2022**, *6* (5), e400–e409. https://doi.org/10.1016/S2542-5196(22)00067-5.
(14) Wang, S.; Gallimore, P. J.; Liu-Kang, C.; Yeung, K.; Campbell, S. J.; Utinger, B.; Liu, T.; Peng, H.; Kalberer, M.; Chan, A. W. H.; Abbatt, J. P. D. Dynamic Wood Smoke Aerosol Toxicity during Oxidative Atmospheric Aging. *Environ. Sci. Technol.* **2023**, *57* (3), 1246–1256. https://doi.org/10.1021/acs.est.2c05929.
(15) Pardo, M.; Li, C.; He, Q.; Levin-Zaidman, S.; Tsoory, M.; Yu, Q.; Wang, X.; Rudich, Y. Mechanisms of Lung Toxicity Induced by Biomass Burning Aerosols. *Part. Fibre Toxicol.* **2020**, *17*, 4. https://doi.org/10.1186/s12989-020-0337-x.
(16) Zhang, Y.; Forrister, H.; Liu, J.; DIbb, J.; Anderson, B.; Schwarz, J. P.; Perring, A. E.; Jimenez, J. L.; Campuzano-Jost, P.; Wang, Y.; Nenes, A.; Weber, R. J. Top-of-Atmosphere Radiative Forcing Affected by Brown Carbon in the Upper Troposphere. *Nat. Geosci.* **2017**, *10* (7), 486–489. https://doi.org/10.1038/ngeo2960.
(17) Brown, H.; Liu, X.; Pokhrel, R.; Murphy, S.; Lu, Z.; Saleh, R.; Mielonen, T.; Kokkola, H.; Bergman, T.; Myhre, G.; Skeie, R. B.; Watson-Paris, D.; Stier, P.; Johnson, B.; Bellouin, N.; Schulz, M.; Vakkari, V.; Beukes, J. P.; van Zyl, P. G.; Liu, S.; Chand, D. Biomass Burning Aerosols in Most Climate Models Are Too Absorbing. *Nat. Commun.* **2021**, *12* (1), 277–277. https://doi.org/10.1038/s41467-020-20482-9.
(18) Yue, S.; Zhu, J.; Chen, S.; Xie, Q.; Li, W.; Li, L.; Ren, H.; Su, S.; Li, P.; Ma, H.; Fan, Y.; Cheng, B.; Wu, L.; Deng, J.; Hu, W.; Ren, L.; Wei, L.; Zhao, W.; Tian, Y.; Pan, X.; Sun, Y.; Wang, Z.; Wu, F.; Liu, C.-Q.; Su, H.; Penner, J. E.; Pöschl, U.; Andreae, M. O.; Cheng, Y.; Fu, P. Brown Carbon from Biomass Burning Imposes Strong Circum-Arctic Warming. *One Earth* **2022**, *5* (3), 293–304. https://doi.org/10.1016/j.oneear.2022.02.006.
(19) Saleh, R. From Measurements to Models: Toward Accurate Representation of Brown Carbon in Climate Calculations. *Curr. Pollut. Rep.* **2020**, *6* (2), 90–104. https://doi.org/10.1007/s40726-020-00139-3.
(20) Chung, C. E.; Ramanathan, V.; Decremer, D. Observationally Constrained Estimates of Carbonaceous Aerosol Radiative Forcing. *Proc. Natl. Acad. Sci. U. S. A.* **2012**, *109* (29), 11624–11629. https://doi.org/10.1073/pnas.1203707109.
(21) Carrico, C. M.; Petters, M. D.; Kreidenweiss, S. M.; Collett, J. L.; Engling, G.; Malm, W. C. Aerosol Hygroscopicity and Cloud Droplet Activation of Extracts of Filters from

https://doi.org/10.26434/chemrxiv-2024-5p8pn-v2 **ORCID:** https://orcid.org/0000-0002-5621-2323 Content not peer-reviewed by ChemRxiv. **License:** CC BY 4.0

Biomass Burning Experiments. *J. Geophys. Res. Atmospheres* **2008**, *113* (8). https://doi.org/10.1029/2007JD009274.
(22) Knopf, D. A.; Alpert, P. A.; Wang, B. The Role of Organic Aerosol in Atmospheric Ice Nucleation: A Review. *ACS Earth Space Chem.* **2018**, *2* (3), 168–202. https://doi.org/10.1021/acsearthspacechem.7b00120.
(23) Bougiatioti, A.; Bezantakos, S.; Stavroulas, I.; Kalivitis, N.; Kokkalis, P.; Biskos, G.; Mihalopoulos, N.; Papayannis, A.; Nenes, A. Biomass-Burning Impact on CCN Number, Hygroscopicity and Cloud Formation during Summertime in the Eastern Mediterranean. *Atmospheric Chem. Phys.* **2016**, *16* (11), 7389–7409. https://doi.org/10.5194/acp-16-7389-2016.
(24) Liu, Y.; Stanturf, J.; Goodrick, S. Trends in Global Wildfire Potential in a Changing Climate. *For. Ecol. Manag.* **2010**, *259* (4), 685–697. https://doi.org/10.1016/j.foreco.2009.09.002.
(25) Liu, Y.; L. Goodrick, S.; A. Stanturf, J. Future U.S. Wildfire Potential Trends Projected Using a Dynamically Downscaled Climate Change Scenario. *For. Ecol. Manag.* **2013**, *294*, 120–135. https://doi.org/10.1016/j.foreco.2012.06.049.
(26) de Groot, W. J.; Flannigan, M. D.; Cantin, A. S. Climate Change Impacts on Future Boreal Fire Regimes. *For. Ecol. Manag.* **2013**, *294*, 35–44. https://doi.org/10.1016/j.foreco.2012.09.027.
(27) Abram, N. J.; Henley, B. J.; Sen Gupta, A.; Lippmann, T. J. R.; Clarke, H.; Dowdy, A. J.; Sharples, J. J.; Nolan, R. H.; Zhang, T.; Wooster, M. J.; Wurtzel, J. B.; Meissner, K. J.; Pitman, A. J.; Ukkola, A. M.; Murphy, B. P.; Tapper, N. J.; Boer, M. M. Connections of Climate Change and Variability to Large and Extreme Forest Fires in Southeast Australia. *Commun. Earth Environ.* **2021**, *2* (1), 8. https://doi.org/10.1038/s43247-020-00065-8.
(28) Song, M.; Marcolli, C.; Krieger, U. K.; Zuend, A.; Peter, T. Liquid-Liquid Phase Separation in Aerosol Particles: Dependence on O:C, Organic Functionalities, and Compositional Complexity. *Geophys. Res. Lett.* **2012**, *39* (19), 1–5. https://doi.org/10.1029/2012GL052807.
(29) Zuend, A.; Marcolli, C.; Peter, T.; Seinfeld, J. H. Computation of Liquid-Liquid Equilibria and Phase Stabilities: Implications for RH-Dependent Gas/Particle Partitioning of Organic-Inorganic Aerosols. *Atmospheric Chem. Phys.* **2010**, *10* (16), 7795–7820. https://doi.org/10.5194/acp-10-7795-2010.
(30) Zuend, A.; Seinfeld, J. H. Modeling the Gas-Particle Partitioning of Secondary Organic Aerosol: The Importance of Liquid-Liquid Phase Separation. *Atmospheric Chem. Phys.* **2012**, *12* (9), 3857–3882. https://doi.org/10.5194/acp-12-3857-2012.
(31) Liu, P.; Song, M.; Zhao, T.; Gunthe, S. S.; Ham, S.; He, Y.; Qin, Y. M.; Gong, Z.; Amorim, J. C.; Bertram, A. K.; Martin, S. T. Resolving the Mechanisms of Hygroscopic Growth and Cloud Condensation Nuclei Activity for Organic Particulate Matter. *Nat. Commun.* **2018**, *9* (1), 4076. https://doi.org/10.1038/s41467-018-06622-2.
(32) Renbaum-Wolff, L.; Song, M.; Marcolli, C.; Zhang, Y.; Liu, P. F.; Grayson, J. W.; Geiger, F. M.; Martin, S. T.; Bertram, A. K. Observations and Implications of Liquid–Liquid Phase Separation at High Relative Humidities in Secondary Organic Material Produced by α-Pinene Ozonolysis without Inorganic Salts. *Atmospheric Chem. Phys.* **2016**, *16* (12), 7969–7979. https://doi.org/10.5194/acp-16-7969-2016.
(33) Ovadnevaite, J.; Zuend, A.; Laaksonen, A.; Sanchez, K. J.; Roberts, G.; Ceburnis, D.; Decesari, S.; Rinaldi, M.; Hodas, N.; Facchini, M. C.; Seinfeld, J. H.; C, O. D. Surface

https://doi.org/10.26434/chemrxiv-2024-5p8pn-v2 **ORCID:** https://orcid.org/0000-0002-5621-2323 Content not peer-reviewed by ChemRxiv. **License:** CC BY 4.0

Tension Prevails over Solute Effect in Organic-Influenced Cloud Droplet Activation. *Nature* **2017**, *546* (7660), 637–641. https://doi.org/10.1038/nature22806.
(34) Gregson, F. K. A.; Gerrebos, N. G. A.; Schervish, M.; Nikkho, S.; Schnitzler, E. G.; Schwartz, C.; Carlsten, C.; Abbatt, J. P. D.; Kamal, S.; Shiraiwa, M.; Bertram, A. K. Phase Behavior and Viscosity in Biomass Burning Organic Aerosol and Climatic Impacts. *Environ. Sci. Technol.* **2023**, *57* (39), 14548–14557. https://doi.org/10.1021/acs.est.3c03231.
(35) Schnitzler, E. G.; Gerrebos, N. G. A.; Carter, T. S.; Huang, Y.; Heald, C. L.; Bertram, A. K.; Abbatt, J. P. D. Rate of Atmospheric Brown Carbon Whitening Governed by Environmental Conditions. *Proc. Natl. Acad. Sci.* **2022**, *119* (38). https://doi.org/10.1073/pnas.2205610119.
(36) Schmedding, R.; Ma, M. T.; Zhang, Y.; Farrell, S.; Pye, H. O. T.; Chen, Y. Z.; Wang, C. T.; Rasool, Q. Z.; Budisulistiorini, S. H.; Ault, A. P.; Surratt, J. D.; Vizuete, W. Alpha-Pinene-Derived Organic Coatings on Acidic Sulfate Aerosol Impacts Secondary Organic Aerosol Formation from Isoprene in a Box Model. *Atmos. Environ.* **2019**, *213*, 456–462. https://doi.org/10.1016/j.atmosenv.2019.06.005.
(37) Zhang, Y.; Chen, Y.; Lambe, A. T.; Olson, N. E.; Lei, Z.; Craig, R. L.; Zhang, Z.; Gold, A.; Onasch, T. B.; Jayne, J. T.; Worsnop, D. R.; Gaston, C. J.; Thornton, J. A.; Vizuete, W.; Ault, A. P.; Surratt, J. D. Effect of the Aerosol-Phase State on Secondary Organic Aerosol Formation from the Reactive Uptake of Isoprene-Derived Epoxydiols (IEPOX). *Environ. Sci. Technol. Lett.* **2018**, *5* (3), 167–174. https://doi.org/10.1021/acs.estlett.8b00044.
(38) Rasool, Q. Z.; Shrivastava, M.; Liu, Y.; Gaudet, B.; Zhao, B. Modeling the Impact of the Organic Aerosol Phase State on Multiphase OH Reactive Uptake Kinetics and the Resultant Heterogeneous Oxidation Timescale of Organic Aerosol in the Amazon Rainforest. *ACS Earth Space Chem.* **2023**, *7* (5), 1009–1024. https://doi.org/10.1021/acsearthspacechem.2c00366.
(39) Schnitzler, E. G.; Abbatt, J. P. D. Heterogeneous OH Oxidation of Secondary Brown Carbon Aerosol. *Atmospheric Chem. Phys.* **2018**, *18* (19), 14539–14553. https://doi.org/10.5194/acp-18-14539-2018.
(40) Alpert, P. A.; Arroyo, P. C.; Dou, J.; Krieger, U. K.; Steimer, S. S.; Förster, J.-D.; Ditas, F.; Pöhlker, C.; Rossignol, S.; Passananti, M.; Perrier, S.; George, C.; Shiraiwa, M.; Berkemeier, T.; Watts, B.; Ammann, M. Visualizing Reaction and Diffusion in Xanthan Gum Aerosol Particles Exposed to Ozone. *Phys. Chem. Chem. Phys.* **2019**, *21* (37), 20613–20627. https://doi.org/10.1039/C9CP03731D.
(41) Li, J.; Forrester, S. M.; Knopf, D. A. Heterogeneous Oxidation of Amorphous Organic Aerosol Surrogates by O_3, NO_3, and OH at Typical Tropospheric Temperatures. *Atmospheric Chem. Phys.* **2020**, *20* (10), 6055–6080. https://doi.org/10.5194/acp-20-6055-2020.
(42) Kiland, K. J.; Mahrt, F.; Peng, L.; Nikkho, S.; Zaks, J.; Crescenzo, G. V.; Bertram, A. K. Viscosity, Glass Formation, and Mixing Times within Secondary Organic Aerosol from Biomass Burning Phenolics. *ACS Earth Space Chem.* **2023**, *7* (7), 1388–1400. https://doi.org/10.1021/acsearthspacechem.3c00039.
(43) Xu, W.; Li, Z.; Zhang, Z.; Li, J.; Karnezi, E.; Lambe, A. T.; Zhou, W.; Sun, J.; Du, A.; Li, Y.; Sun, Y. Changes in Physicochemical Properties of Organic Aerosol During Photochemical Aging of Cooking and Burning Emissions. *J. Geophys. Res. Atmospheres* **2023**, *128* (14), e2022JD037911. https://doi.org/10.1029/2022JD037911.

https://doi.org/10.26434/chemrxiv-2024-5p8pn-v2 **ORCID:** https://orcid.org/0000-0002-5621-2323 Content not peer-reviewed by ChemRxiv. **License:** CC BY 4.0

(44) Jahn, L. G.; Jahl, L. G.; Bowers, B. B.; Sullivan, R. C. Morphology of Organic Carbon Coatings on Biomass-Burning Particles and Their Role in Reactive Gas Uptake. *ACS Earth Space Chem.* **2021**, *5* (9), 2184–2195. https://doi.org/10.1021/acsearthspacechem.1c00237.
(45) Hettiyadura, A. P. S.; Garcia, V.; Li, C.; West, C. P.; Tomlin, J.; He, Q.; Rudich, Y.; Laskin, A. Chemical Composition and Molecular-Specific Optical Properties of Atmospheric Brown Carbon Associated with Biomass Burning. *Environ. Sci. Technol.* **2021**, *55* (4), 2511–2521. https://doi.org/10.1021/acs.est.0c05883.
(46) Li, C.; He, Q.; Schade, J.; Passig, J.; Zimmermann, R.; Meidan, D.; Laskin, A.; Rudich, Y. Dynamic Changes in Optical and Chemical Properties of Tar Ball Aerosols by Atmospheric Photochemical Aging. *Atmospheric Chem. Phys.* **2019**, *19* (1), 139–163. https://doi.org/10.5194/acp-19-139-2019.
(47) China, S.; Mazzoleni, C.; Gorkowski, K.; Aiken, A. C.; Dubey, M. K. Morphology and Mixing State of Individual Freshly Emitted Wildfire Carbonaceous Particles. *Nat. Commun.* **2013**, *4* (1), 2122–2128. https://doi.org/10.1038/ncomms3122.
(48) Hand, J. L.; Malm, W. C.; Laskin, A.; Day, D.; Lee, T.; Wang, C.; Carrico, C.; Carrillo, J.; Cowin, J. P.; Collett Jr., J.; Iedema, M. J. Optical, Physical, and Chemical Properties of Tar Balls Observed during the Yosemite Aerosol Characterization Study. *J. Geophys. Res. Atmospheres* **2005**, *110* (D21). https://doi.org/10.1029/2004JD005728.
(49) Tivanski, A. V.; Hopkins, R. J.; Tyliszczak, T.; Gilles, M. K. Oxygenated Interface on Biomass Burn Tar Balls Determined by Single Particle Scanning Transmission X-Ray Microscopy. *J. Phys. Chem. A* **2007**, *111* (25), 5448–5458. https://doi.org/10.1021/jp070155u.
(50) Al-Mashala, H. H.; Betz, K. L.; Calvert, C. T.; Barton, J. A.; Bruce, E. E.; Schnitzler, E. G. Ultraviolet Irradiation Can Increase the Light Absorption and Viscosity of Primary Brown Carbon from Biomass Burning. *ACS Earth Space Chem.* **2023**, *7* (10), 1882–1889. https://doi.org/10.1021/acsearthspacechem.3c00155.
(51) Feng, T.; Wang, Y.; Hu, W.; Zhu, M.; Song, W.; Chen, W.; Sang, Y.; Fang, Z.; Deng, W.; Fang, H.; Yu, X.; Wu, C.; Yuan, B.; Huang, S.; Shao, M.; Huang, X.; He, L.; Lee, Y. R.; Huey, L. G.; Canonaco, F.; Prevot, A. S. H.; Wang, X. Impact of Aging on the Sources, Volatility, and Viscosity of Organic Aerosols in Chinese Outflows. *Atmospheric Chem. Phys.* **2023**, *23* (1), 611–636. https://doi.org/10.5194/acp-23-611-2023.
(52) Mahrt, F.; Newman, E.; Huang, Y.; Ammann, M.; Bertram, A. K. Phase Behavior of Hydrocarbon-like Primary Organic Aerosol and Secondary Organic Aerosol Proxies Based on Their Elemental Oxygen-to-Carbon Ratio. *Environ. Sci. Technol.* **2021**. https://doi.org/10.1021/acs.est.1c02697.
(53) Mahrt, F.; Peng, L.; Zaks, J.; Huang, Y.; Ohno, P. E.; Smith, N. R.; Gregson, F. K. A.; Qin, Y.; Faiola, C. L.; Martin, S. T.; Nizkorodov, S. A.; Ammann, M.; Bertram, A. K. Not All Types of Secondary Organic Aerosol Mix: Two Phases Observed When Mixing Different Secondary Organic Aerosol Types. *Atmospheric Chem. Phys.* **2022**, *22* (20), 13783–13796. https://doi.org/10.5194/acp-22-13783-2022.
(54) Song, M.; Marcolli, C.; Krieger, U. K.; Zuend, A.; Peter, T. Liquid-Liquid Phase Separation in Aerosol Particles: Dependence on O:C, Organic Functionalities, and Compositional Complexity. *Geophys. Res. Lett.* **2012**, *39* (19), 1–5. https://doi.org/10.1029/2012GL052807.
(55) Schmedding, R.; Rasool, Q. Z.; Zhang, Y.; Pye, H. O. T.; Zhang, H.; Chen, Y.; Surratt, J. D.; Lopez-Hilfiker, F. D.; Thornton, J. A.; Goldstein, A. H.; Vizuete, W. Predicting

https://doi.org/10.26434/chemrxiv-2024-5p8pn-v2 **ORCID:** https://orcid.org/0000-0002-5621-2323 Content not peer-reviewed by ChemRxiv. **License:** CC BY 4.0

Secondary Organic Aerosol Phase State and Viscosity and Its Effect on Multiphase Chemistry in a Regional-Scale Air Quality Model. *Atmospheric Chem. Phys.* **2020**, *20* (13), 8201–8225. https://doi.org/10.5194/acp-20-8201-2020.
(56) Mahrt, F.; Huang, Y.; Zaks, J.; Devi, A.; Peng, L.; Ohno, P. E.; Qin, Y. M.; Martin, S. T.; Ammann, M.; Bertram, A. K. Phase Behavior of Internal Mixtures of Hydrocarbon-like Primary Organic Aerosol and Secondary Aerosol Based on Their Differences in Oxygen-to-Carbon Ratios. *Environ. Sci. Technol.* **2022**, *56* (7), 3960–3973. https://doi.org/10.1021/acs.est.1c07691.
(57) Gorkowski, K.; Donahue, N. M.; Sullivan, R. C. Aerosol Optical Tweezers Constrain the Morphology Evolution of Liquid-Liquid Phase-Separated Atmospheric Particles. *Chem* **2020**, *6* (1), 204–220. https://doi.org/10.1016/j.chempr.2019.10.018.
(58) Hodshire, A. L.; Akherati, A.; Alvarado, M. J.; Brown-Steiner, B.; Jathar, S. H.; Jimenez, J. L.; Kreidenweis, S. M.; Lonsdale, C. R.; Onasch, T. B.; Ortega, A. M.; Pierce, J. R. Aging Effects on Biomass Burning Aerosol Mass and Composition: A Critical Review of Field and Laboratory Studies. *Environ. Sci. Technol.* **2019**, *53* (17), 10007–10022. https://doi.org/10.1021/acs.est.9b02588.
(59) Ortega, A. M.; Day, D. A.; Cubison, M. J.; Brune, W. H.; Bon, D.; de Gouw, J. A.; Jimenez, J. L. Secondary Organic Aerosol Formation and Primary Organic Aerosol Oxidation from Biomass-Burning Smoke in a Flow Reactor during FLAME-3. *Atmospheric Chem. Phys.* **2013**, *13* (22), 11551–11571. https://doi.org/10.5194/acp-13-11551-2013.
(60) Pósfai, M.; Gelencsér, A.; Simonics, R.; Arató, K.; Li, J.; Hobbs, P. V.; Buseck, P. R. Atmospheric Tar Balls: Particles from Biomass and Biofuel Burning. *J. Geophys. Res. Atmospheres* **2004**, *109* (D6). https://doi.org/10.1029/2003JD004169.
(61) Tóth, A.; Hoffer, A.; Nyirő-Kósa, I.; Pósfai, M.; Gelencsér, A. Atmospheric Tar Balls: Aged Primary Droplets from Biomass Burning? *Atmospheric Chem. Phys.* **2014**, *14* (13), 6669–6675. https://doi.org/10.5194/acp-14-6669-2014.
(62) Adachi, K.; Dibb, J. E.; Katich, J. M.; Schwarz, J. P.; Guo, H.; Campuzano-Jost, P.; Jimenez, J. L.; Peischl, J.; Holmes, C. D.; Crawford, J. Occurrence, Abundance, and Formation of Atmospheric Tarballs from a Wide Range of Wildfires in the Western US. *EGUsphere* **2024**, 1–30. https://doi.org/10.5194/egusphere-2024-880.
(63) Adachi, K.; Buseck, P. R. Atmospheric Tar Balls from Biomass Burning in Mexico. *J. Geophys. Res. Atmospheres* **2011**, *116* (D5). https://doi.org/10.1029/2010JD015102.
(64) Reid, J. P.; Bertram, A. K.; Topping, D. O.; Laskin, A.; Martin, S. T.; Petters, M. D.; Pope, F. D.; Rovelli, G. The Viscosity of Atmospherically Relevant Organic Particles. *Nat. Commun.* **2018**, *9* (1), 956. https://doi.org/10.1038/s41467-018-03027-z.
(65) Adachi, K.; Sedlacek III, A. J.; Kleinman, L.; Chand, D.; Hubbe, J. M.; Buseck, P. R. Volume Changes upon Heating of Aerosol Particles from Biomass Burning Using Transmission Electron Microscopy. *Aerosol Sci. Technol.* **2018**, *52* (1), 46–56. https://doi.org/10.1080/02786826.2017.1373181.
(66) Sedlacek III, A. J.; Buseck, P. R.; Adachi, K.; Onasch, T. B.; Springston, S. R.; Kleinman, L. Formation and Evolution of Tar Balls from Northwestern US Wildfires. *Atmospheric Chem. Phys.* **2018**, *18* (15), 11289–11301. https://doi.org/10.5194/acp-18-11289-2018.
(67) British Columbia Ministry of Environment. *Envista - Air Resources Manager*. B.C. Air Data Archive. https://envistaweb.env.gov.bc.ca/ (accessed 2024-04-09).
(68) NASA. *FIRMS US/CANADA*. https://firms.modaps.eosdis.nasa.gov/map/ (accessed 2024-04-09).

https://doi.org/10.26434/chemrxiv-2024-5p8pn-v2 **ORCID:** https://orcid.org/0000-0002-5621-2323 Content not peer-reviewed by ChemRxiv. **License:** CC BY 4.0

(69) Wulder, M. A. *BC Tree Species Map/Likelihoods 2015 - Open Government Portal*. https://open.canada.ca/data/en/dataset/8dddaa7f-c60d-4802-a662-2930c5aeedb8 (accessed 2024-03-01).
(70) Hamann, A.; Smets, P.; Yanchuk, A. D.; Aitken, S. N. An Ecogeographic Framework for in Situ Conservation of Forest Trees in British Columbia. *Can. J. For. Res.* **2005**, *35* (11), 2553–2561. https://doi.org/10.1139/x05-181.
(71) Rolph, G.; Stein, A.; Stunder, B. Real-Time Environmental Applications and Display sYstem: READY. *Environ. Model. Softw.* **2017**, *95*, 210–228. https://doi.org/10.1016/j.envsoft.2017.06.025.
(72) NOAA Air Resources Laboratory. *READY - Real-time Environmental Applications and Display sYstem*. https://www.ready.noaa.gov/index.php (accessed 2024-04-09).
(73) Hems, R. F.; Schnitzler, E. G.; Bastawrous, M.; Soong, R.; Simpson, A. J.; Abbatt, J. P. D. Aqueous Photoreactions of Wood Smoke Brown Carbon. *ACS Earth Space Chem.* **2020**, *4* (7), 1149–1160. https://doi.org/10.1021/acsearthspacechem.0c00117.
(74) Trofimova, A.; Hems, R. F.; Liu, T.; Abbatt, J. P. D.; Schnitzler, E. G. Contribution of Charge-Transfer Complexes to Absorptivity of Primary Brown Carbon Aerosol. *ACS Earth Space Chem.* **2019**, *3* (8), 1393–1401. https://doi.org/10.1021/acsearthspacechem.9b00116.
(75) Greenspan, L. Humidity Fixed Points of Binary Saturated Aqueous Solutions. *J. Res. Natl. Bur. Stand. Sect. Phys. Chem.* **1977**, *81* (1), 89–96.
(76) Parsons, M. T.; Mak, J.; Lipetz, S. R.; Bertram, A. K. Deliquescence of Malonic, Succinic, Glutaric, and Adipic Acid Particles. *J. Geophys. Res. Atmospheres* **2004**, *109* (D6). https://doi.org/10.1029/2003JD004075.
(77) Murray, B. J.; Haddrell, A. E.; Peppe, S.; Davies, J. F.; Reid, J. P.; O'Sullivan, D.; Price, H. C.; Kumar, R.; Saunders, R. W.; Plane, J. M. C.; Umo, N. S.; Wilson, T. W. Glass Formation and Unusual Hygroscopic Growth of Iodic Acid Solution Droplets with Relevance for Iodine Mediated Particle Formation in the Marine Boundary Layer. *Atmospheric Chem. Phys.* **2012**, *12* (18), 8575–8587. https://doi.org/10.5194/acp-12-8575-2012.
(78) Renbaum-Wolff, L.; Grayson, J. W.; Bateman, A. P.; Kuwata, M.; Sellier, M.; Murray, B. J.; Shilling, J. E.; Martin, S. T.; Bertram, A. K. Viscosity of α-Pinene Secondary Organic Material and Implications for Particle Growth and Reactivity. *Proc. Natl. Acad. Sci. U. S. A.* **2013**, *110* (20), 8014–8019. https://doi.org/10.1073/pnas.1219548110.
(79) Grayson, J. W.; Song, M.; Sellier, M.; Bertram, A. K. Validation of the Poke-Flow Technique Combined with Simulations of Fluid Flow for Determining Viscosities in Samples with Small Volumes and High Viscosities. *Atmospheric Meas. Tech.* **2015**, *8* (6), 2463–2472. https://doi.org/10.5194/amt-8-2463-2015.
(80) Smith, N. R.; Crescenzo, G. V.; Bertram, A. K.; Nizkorodov, S. A.; Faiola, C. L. Insect Infestation Increases Viscosity of Biogenic Secondary Organic Aerosol. *ACS Earth Space Chem.* **2023**, *7* (5), 1060–1071. https://doi.org/10.1021/acsearthspacechem.3c00007.
(81) Smith, N. R.; Crescenzo, G. V.; Huang, Y.; Hettiyadura, A. P. S.; Siemens, K.; Li, Y.; Faiola, C. L.; Laskin, A.; Shiraiwa, M.; Bertram, A. K.; Nizkorodov, S. A. Viscosity and Liquid–Liquid Phase Separation in Healthy and Stressed Plant SOA. *Environ. Sci. Atmospheres* **2021**, *1* (3), 140–153. https://doi.org/10.1039/D0EA00020E.
(82) Song, M.; Jeong, R.; Kim, D.; Qiu, Y.; Meng, X.; Wu, Z.; Zuend, A.; Ha, Y.; Kim, C.; Kim, H.; Gaikwad, S.; Jang, K. S.; Lee, J. Y.; Ahn, J. Comparison of Phase States of PM(2.5) over Megacities, Seoul and Beijing, and Their Implications on Particle Size

https://doi.org/10.26434/chemrxiv-2024-5p8pn-v2 **ORCID:** https://orcid.org/0000-0002-5621-2323 Content not peer-reviewed by ChemRxiv. **License:** CC BY 4.0

Distribution. *Env. Sci Technol* **2022**, *56* (24), 17581–17590. https://doi.org/10.1021/acs.est.2c06377.
(83) Gaikwad, S.; Jeong, R.; Kim, D.; Lee, K.; Jang, K.-S.; Kim, C.; Song, M. Microscopic Observation of a Liquid-Liquid-(Semi)Solid Phase in Polluted PM2.5. *Front. Environ. Sci.* **2022**, *10*. https://doi.org/10.3389/fenvs.2022.947924.
(84) DeCarlo, P. F.; Kimmel, J. R.; Trimborn, A.; Northway, M. J.; Jayne, J. T.; Aiken, A. C.; Gonin, M.; Fuhrer, K.; Horvath, T.; Docherty, K. S.; Worsnop, D. R.; Jimenez, J. L. Field-Deployable, High-Resolution, Time-of-Flight Aerosol Mass Spectrometer. *Anal. Chem.* **2006**, *78* (24), 8281–8289. https://doi.org/10.1021/ac061249n.
(85) Aiken, A. C.; Decarlo, P. F.; Kroll, J. H.; Worsnop, D. R.; Huffman, J. A.; Docherty, K. S.; Ulbrich, I. M.; Mohr, C.; Kimmel, J. R.; Sueper, D.; Sun, Y.; Zhang, Q.; Trimborn, A.; Northway, M.; Ziemann, P. J.; Canagaratna, M. R.; Onasch, T. B.; Alfarra, M. R.; Prevot, A. S. H.; Dommen, J.; Duplissy, J.; Metzger, A.; Baltensperger, U.; Jimenez, J. L. O/C and OM/OC Ratios of Primary, Secondary, and Ambient Organic Aerosols with High-Resolution Time-of-Flight Aerosol Mass Spectrometry. *Environ. Sci. Technol.* **2008**, *42* (12), 4478--4485. https://doi.org/10.1021/es703009q.
(86) Aiken, A. C.; DeCarlo, P. F.; Jimenez, J. L. Elemental Analysis of Organic Species with Electron Ionization High-Resolution Mass Spectrometry. *Anal. Chem.* **2007**, *79* (21), 8350–8358. https://doi.org/10.1021/ac071150w.
(87) Canagaratna, M. R.; Jimenez, J. L.; Kroll, J. H.; Chen, Q.; Kessler, S. H.; Massoli, P.; Hildebrandt Ruiz, L.; Fortner, E.; Williams, L. R.; Wilson, K. R.; Surratt, J. D.; Donahue, N. M.; Jayne, J. T.; Worsnop, D. R. Elemental Ratio Measurements of Organic Compounds Using Aerosol Mass Spectrometry: Characterization, Improved Calibration, and Implications. *Atmospheric Chem. Phys.* **2015**, *15* (1), 253–272. https://doi.org/10.5194/acp-15-253-2015.
(88) Kroll, J. H.; Donahue, N. M.; Jimenez, J. L.; Kessler, S. H.; Canagaratna, M. R.; Wilson, K. R.; Altieri, K. E.; Mazzoleni, L. R.; Wozniak, A. S.; Bluhm, H.; Mysak, E. R.; Smith, J. D.; Kolb, C. E.; Worsnop, D. R. Carbon Oxidation State as a Metric for Describing the Chemistry of Atmospheric Organic Aerosol. *Nat. Chem.* **2011**, *3* (2), 133–139. https://doi.org/10.1038/nchem.948.
(89) Lim, C. Y.; Hagan, D. H.; Coggon, M. M.; Koss, A. R.; Sekimoto, K.; de Gouw, J.; Warneke, C.; Cappa, C. D.; Kroll, J. H. Secondary Organic Aerosol Formation from the Laboratory Oxidation of Biomass Burning Emissions. *Atmospheric Chem. Phys.* **2019**, *19* (19), 12797–12809. https://doi.org/10.5194/acp-19-12797-2019.
(90) DeRieux, W.-S. W.; Li, Y.; Lin, P.; Laskin, J.; Laskin, A.; Bertram, A. K.; Nizkorodov, S. A.; Shiraiwa, M. Predicting the Glass Transition Temperature and Viscosity of Secondary Organic Material Using Molecular Composition. *Atmospheric Chem. Phys.* **2018**, *18* (9), 6331–6351. https://doi.org/10.5194/acp-18-6331-2018.
(91) You, Y.; Smith, M. L.; Song, M.; Martin, S. T.; Bertram, A. K. Liquid–Liquid Phase Separation in Atmospherically Relevant Particles Consisting of Organic Species and Inorganic Salts. *Int. Rev. Phys. Chem.* **2014**, *33* (1), 43–77. https://doi.org/10.1080/0144235X.2014.890786.
(92) Freedman, M. A. Phase Separation in Organic Aerosol. *Chem. Soc. Rev.* **2017**, *46* (24), 7694–7705. https://doi.org/10.1039/c6cs00783j.
(93) Reid, J. P.; Dennis-Smither, B. J.; Kwamena, N.-O. A.; Miles, R. E. H.; Hanford, K. L.; Homer, C. J. The Morphology of Aerosol Particles Consisting of Hydrophobic and

https://doi.org/10.26434/chemrxiv-2024-5p8pn-v2 **ORCID:** https://orcid.org/0000-0002-5621-2323 Content not peer-reviewed by ChemRxiv. **License:** CC BY 4.0

Hydrophilic Phases: Hydrocarbons, Alcohols and Fatty Acids as the Hydrophobic Component. *Phys. Chem. Chem. Phys.* **2011**, *13* (34), 15559–15572. https://doi.org/10.1039/C1CP21510H.

(94) Rana, A.; Dey, S.; Sarkar, S. Chapter 16 - Optical Properties of Brown Carbon in Aerosols and Surface Snow at Ny-Ålesund during the Polar Summer. In *Understanding Present and Past Arctic Environments*; Khare, N., Ed.; Elsevier, 2021; pp 343–356. https://doi.org/10.1016/B978-0-12-822869-2.00022-0.

(95) Mikhailov, E.; Vlasenko, S.; Martin, S. T.; Koop, T.; Pöschl, U. Amorphous and Crystalline Aerosol Particles Interacting with Water Vapor: Conceptual Framework and Experimental Evidence for Restructuring, Phase Transitions and Kinetic Limitations. *Atmospheric Chem. Phys.* **2009**, *9* (24), 9491–9522. https://doi.org/10.5194/acp-9-9491-2009.

(96) Grunberg, L.; Nissan, A. H. Mixture Law for Viscosity. *Nature* **1949**, *164* (4175), 799–800. https://doi.org/10.1038/164799b0.

(97) Semeniuk, T. A.; Wise, M. E.; Martin, S. T.; Russell, L. M.; Buseck, P. R. Hygroscopic Behavior of Aerosol Particles from Biomass Fires Using Environmental Transmission Electron Microscopy. *J. Atmospheric Chem.* **2007**, *56* (3), 259–273. https://doi.org/10.1007/s10874-006-9055-5.

(98) Dusek, U.; Frank, G. P.; Helas, G.; Iinuma, Y.; Zeromskiene, K.; Gwaze, P.; Hennig, T.; Massling, A.; Schmid, O.; Herrmann, H.; Wiedensohler, A.; Andreae, M. O. "Missing" Cloud Condensation Nuclei in Peat Smoke. *Geophys. Res. Lett.* **2005**, *32* (11). https://doi.org/10.1029/2005GL022473.

(99) Grayson, J. W.; Evoy, E.; Song, M.; Chu, Y.; Maclean, A.; Nguyen, A.; Upshur, M. A.; Ebrahimi, M.; Chan, C. K.; Geiger, F. M.; Thomson, R. J.; Bertram, A. K. The Effect of Hydroxyl Functional Groups and Molar Mass on the Viscosity of Non-Crystalline Organic and Organic–Water Particles. *Atmospheric Chem. Phys.* **2017**, *17* (13), 8509–8524. https://doi.org/10.5194/acp-17-8509-2017.

(100) Rothfuss, N. E.; Petters, M. D. Characterization of the Temperature and Humidity-Dependent Phase Diagram of Amorphous Nanoscale Organic Aerosols. *Phys. Chem. Chem. Phys.* **2017**, *19* (9), 6532–6545. https://doi.org/10.1039/c6cp08593h.

(101) Koop, T.; Bookhold, J.; Shiraiwa, M.; Pöschl, U. Glass Transition and Phase State of Organic Compounds: Dependency on Molecular Properties and Implications for Secondary Organic Aerosols in the Atmosphere. *Phys. Chem. Chem. Phys.* **2011**, *13* (43), 19238–19255. https://doi.org/10.1039/c1cp22617g.

(102) Siemens, K.; Paik, T.; Li, A.; Rivera-Adorno, F.; Tomlin, J.; Xie, Q.; Chakrabarty, R. K.; Laskin, A. Light Absorption and Chemical Composition of Brown Carbon Organic Aerosol Produced from Burning of Selected Biofuels. *ACS Earth Space Chem.* **2024**. https://doi.org/10.1021/acsearthspacechem.4c00056.

(103) Chakrabarty, R. K.; Moosmüller, H.; Chen, L.-W. A.; Lewis, K.; Arnott, W. P.; Mazzoleni, C.; Dubey, M. K.; Wold, C. E.; Hao, W. M.; Kreidenweis, S. M. Brown Carbon in Tar Balls from Smoldering Biomass Combustion. *Atmospheric Chem. Phys.* **2010**, *10* (13), 6363–6370. https://doi.org/10.5194/acp-10-6363-2010.

(104) Chakrabarty, R. K.; Moosmüller, H.; Garro, M. A.; Arnott, W. P.; Walker, J.; Susott, R. A.; Babbitt, R. E.; Wold, C. E.; Lincoln, E. N.; Hao, W. M. Emissions from the Laboratory Combustion of Wildland Fuels: Particle Morphology and Size. *J. Geophys. Res. Atmospheres* **2006**, *111* (D7). https://doi.org/10.1029/2005JD006659.

https://doi.org/10.26434/chemrxiv-2024-5p8pn-v2 **ORCID:** https://orcid.org/0000-0002-5621-2323 Content not peer-reviewed by ChemRxiv. **License:** CC BY 4.0

(105) Adachi, K.; Sedlacek, A. J.; Kleinman, L.; Springston, S. R.; Wang, J.; Chand, D.; Hubbe, J. M.; Shilling, J. E.; Onasch, T. B.; Kinase, T.; Sakata, K.; Takahashi, Y.; Buseck, P. R. Spherical Tarball Particles Form through Rapid Chemical and Physical Changes of Organic Matter in Biomass-Burning Smoke. *Proc. Natl. Acad. Sci.* **2019**, *116* (39), 19336–19341. https://doi.org/10.1073/pnas.1900129116.

(106) Zhuravleva, T. B.; Nasrtdinov, I. M.; Konovalov, I. B.; Golovushkin, N. A.; Beekmann, M. Impact of the Atmospheric Photochemical Evolution of the Organic Component of Biomass Burning Aerosol on Its Radiative Forcing Efficiency: A Box Model Analysis. *Atmosphere* **2021**, *12* (12), 1555. https://doi.org/10.3390/atmos12121555.

(107) Akherati, A.; He, Y.; Garofalo, L. A.; Hodshire, A. L.; Farmer, D. K.; Kreidenweis, S. M.; Permar, W.; Hu, L.; Fischer, E. V.; Jen, C. N.; Goldstein, A. H.; Levin, E. J. T.; DeMott, P. J.; Campos, T. L.; Flocke, F.; Reeves, J. M.; Toohey, D. W.; Pierce, J. R.; Jathar, S. H. Dilution and Photooxidation Driven Processes Explain the Evolution of Organic Aerosol in Wildfire Plumes. *Environ. Sci. Atmospheres* **2022**, *2* (5), 1000–1022. https://doi.org/10.1039/D1EA00082A.

(108) Patoulias, D.; Kallitsis, E.; Posner, L.; Pandis, S. N. Modeling Biomass Burning Organic Aerosol Atmospheric Evolution and Chemical Aging. *Atmosphere* **2021**, *12* (12), 1638. https://doi.org/10.3390/atmos12121638.

(109) Shrivastava, M.; Zelenyuk, A.; Imre, D.; Easter, R.; Beranek, J.; Zaveri, R. A.; Fast, J. Implications of Low Volatility SOA and Gas-Phase Fragmentation Reactions on SOA Loadings and Their Spatial and Temporal Evolution in the Atmosphere. *J. Geophys. Res. Atmospheres* **2013**, *118* (8), 3328–3342. https://doi.org/10.1002/jgrd.50160.

(110) Shrivastava, M.; Easter, R. C.; Liu, X.; Zelenyuk, A.; Singh, B.; Zhang, K.; Ma, P.-L.; Chand, D.; Ghan, S.; Jimenez, J. L.; Zhang, Q.; Fast, J.; Rasch, P. J.; Tiitta, P. Global Transformation and Fate of SOA: Implications of Low-Volatility SOA and Gas-Phase Fragmentation Reactions. *J. Geophys. Res. Atmospheres* **2015**, *120* (9), 4169–4195. https://doi.org/10.1002/2014JD022563.

(111) Sedlacek, A. J. I.; Lewis, E. R.; Onasch, T. B.; Zuidema, P.; Redemann, J.; Jaffe, D.; Kleinman, L. I. Using the Black Carbon Particle Mixing State to Characterize the Lifecycle of Biomass Burning Aerosols. *Environ. Sci. Technol.* **2022**, *56* (20), 14315–14325. https://doi.org/10.1021/acs.est.2c03851.

(112) Lack, D. A.; Langridge, J. M.; Bahreini, R.; Cappa, C. D.; Middlebrook, A. M.; Schwarz, J. P. Brown Carbon and Internal Mixing in Biomass Burning Particles. *Proc. Natl. Acad. Sci.* **2012**, *109* (37), 14802–14807. https://doi.org/10.1073/pnas.1206575109.

(113) Brunamonti, S.; Krieger, U. K.; Marcolli, C.; Peter, T. Redistribution of Black Carbon in Aerosol Particles Undergoing Liquid-Liquid Phase Separation. *Geophys. Res. Lett.* **2015**, *42* (7), 2532–2539. https://doi.org/10.1002/2014GL062908.

(114) Zhang, J.; Wang, Y. Y.; Teng, X. M.; Liu, L.; Xu, Y. S.; Ren, L. H.; Shi, Z. B.; Zhang, Y.; Jiang, J. K.; Liu, D. T.; Hu, M.; Shao, L. Y.; Chen, J. M.; Martin, S. T.; Zhang, X. Y.; Li, W. J. Liquid-Liquid Phase Separation Reduces Radiative Absorption by Aged Black Carbon Aerosols. *Commun. Earth Environ.* **2022**, *3* (1). https://doi.org/10.1038/s43247-022-00462-1.

(115) Zuend, A.; Marcolli, C.; Peter, T.; Seinfeld, J. H. Computation of Liquid-Liquid Equilibria and Phase Stabilities: Implications for RH-Dependent Gas/Particle Partitioning of Organic-Inorganic Aerosols. *Atmospheric Chem. Phys.* **2010**, *10* (16), 7795–7820. https://doi.org/10.5194/acp-10-7795-2010.

https://doi.org/10.26434/chemrxiv-2024-5p8pn-v2 **ORCID:** https://orcid.org/0000-0002-5621-2323 Content not peer-reviewed by ChemRxiv. **License:** CC BY 4.0

(116) Pye, H. O. T.; Zuend, A.; Fry, J. L.; Isaacman-VanWertz, G.; Capps, S. L.; Appel, K. W.; Foroutan, H.; Xu, L.; Ng, N. L.; Goldstein, A. H. Coupling of Organic and Inorganic Aerosol Systems and the Effect on Gas-Particle Partitioning in the Southeastern US. *Atmospheric Chem. Phys.* **2018**, *18* (1), 357–370. https://doi.org/10.5194/acp-18-357-2018.
(117) Pye, H. O. T.; Murphy, B. N.; Xu, L.; Ng, N. L.; Carlton, A. G.; Guo, H.; Weber, R.; Vasilakos, P.; Appel, K. W.; Budisulistiorini, S. H.; Surratt, J. D.; Nenes, A.; Hu, W.; Jimenez, J. L.; Isaacman-VanWertz, G.; Misztal, P. K.; Goldstein, A. H. On the Implications of Aerosol Liquid Water and Phase Separation for Organic Aerosol Mass. *Atmospheric Chem. Phys.* **2017**, *17* (1), 343–369. https://doi.org/10.5194/acp-17-343-2017.
(118) Ye, J.; Gordon, C. A.; Chan, A. W. H. Enhancement in Secondary Organic Aerosol Formation in the Presence of Preexisting Organic Particle. *Environ. Sci. Technol.* **2016**, *50* (7), 3572–3579. https://doi.org/10.1021/acs.est.5b05512.
(119) Ye, J.; Van Rooy, P.; Adam, C. H.; Jeong, C.-H.; Urch, B.; Cocker, D. R. I.; Evans, G. J.; Chan, A. W. H. Predicting Secondary Organic Aerosol Enhancement in the Presence of Atmospherically Relevant Organic Particles. *ACS Earth Space Chem.* **2018**, *2* (10), 1035–1046. https://doi.org/10.1021/acsearthspacechem.8b00093.
(120) Ruehl, C. R.; Davies, J. F.; Wilson, K. R. An Interfacial Mechanism for Cloud Droplet Formation on Organic Aerosols. *Science* **2016**, *351* (6280), 1447–1450.
(121) Evoy, E.; Kamal, S.; Patey, G. N.; Martin, S. T.; Bertram, A. K. Unified Description of Diffusion Coefficients from Small to Large Molecules in Organic-Water Mixtures. *J. Phys. Chem. A* **2020**, *124* (11), 2301–2308. https://doi.org/10.1021/acs.jpca.9b11271.
(122) Browne, E. C.; Zhang, X.; Franklin, J. P.; Ridley, K. J.; Kirchstetter, T. W.; Wilson, K. R.; Cappa, C. D.; Kroll, J. H. Effect of Heterogeneous Oxidative Aging on Light Absorption by Biomass Burning Organic Aerosol. *Aerosol Sci. Technol.* **2019**, *53* (6), 663–674. https://doi.org/10.1080/02786826.2019.1599321.
(123) Zelenyuk, A.; Imre, D.; Beránek, J.; Abramson, E.; Wilson, J.; Shrivastava, M. Synergy between Secondary Organic Aerosols and Long-Range Transport of Polycyclic Aromatic Hydrocarbons. *Environ. Sci. Technol.* **2012**, *46* (22), 12459–12466. https://doi.org/10.1021/es302743z.
(124) Kim, Y.; Sartelet, K.; Couvidat, F. Modeling the Effect of Non-Ideality, Dynamic Mass Transfer and Viscosity on SOA Formation in a 3-D Air Quality Model. *Atmospheric Chem. Phys.* **2019**, *19* (2), 1241–1261. https://doi.org/10.5194/acp-19-1241-2019.
(125) Zaveri, R. A.; Shilling, J. E.; Zelenyuk, A.; Liu, J.; Bell, D. M.; D'Ambro, E. L.; Gaston, C. J.; Thornton, J. A.; Laskin, A.; Lin, P.; Wilson, J.; Easter, R. C.; Wang, J.; Bertram, A. K.; Martin, S. T.; Seinfeld, J. H.; Worsnop, D. R. Growth Kinetics and Size Distribution Dynamics of Viscous Secondary Organic Aerosol. *Environ. Sci. Technol.* **2018**, *52* (3), 1191–1199. https://doi.org/10.1021/acs.est.7b04623.
(126) Shiraiwa, M.; Seinfeld, J. H. Equilibration Timescale of Atmospheric Secondary Organic Aerosol Partitioning. *Geophys. Res. Lett.* **2012**, *39* (24). https://doi.org/10.1029/2012GL054008.
(127) Yli-Juuti, T.; Pajunoja, A.; Tikkanen, O.-P.; Buchholz, A.; Faiola, C.; Väisänen, O.; Hao, L.; Kari, E.; Peräkylä, O.; Garmash, O.; Shiraiwa, M.; Ehn, M.; Lehtinen, K.; Virtanen, A. Factors Controlling the Evaporation of Secondary Organic Aerosol from α-Pinene Ozonolysis. *Geophys. Res. Lett.* **2017**, *44* (5), 2562–2570. https://doi.org/10.1002/2016GL072364.

https://doi.org/10.26434/chemrxiv-2024-5p8pn-v2 **ORCID:** https://orcid.org/0000-0002-5621-2323 Content not peer-reviewed by ChemRxiv. **License:** CC BY 4.0

(128) Wall, A. C. V.; Perraud, V.; Wingen, L. M.; Finlayson-Pitts, B. J. Evidence for a Kinetically Controlled Burying Mechanism for Growth of High Viscosity Secondary Organic Aerosol. *Environ. Sci. Process. Impacts* **2020**, *22* (1), 66–83. https://doi.org/10.1039/C9EM00379G.

(129) Wolf, M. J.; Zhang, Y.; Zawadowicz, M. A.; Goodell, M.; Froyd, K.; Freney, E.; Sellegri, K.; Rösch, M.; Cui, T.; Winter, M.; Lacher, L.; Axisa, D.; DeMott, P. J.; Levin, E. J. T.; Gute, E.; Abbatt, J.; Koss, A.; Kroll, J. H.; Surratt, J. D.; Cziczo, D. J. A Biogenic Secondary Organic Aerosol Source of Cirrus Ice Nucleating Particles. *Nat. Commun.* **2020**, *11* (1). https://doi.org/10.1038/s41467-020-18424-6.

(130) Murray, B. J.; Wilson, T. W.; Dobbie, S.; Cui, Z.; Al-Jumur, S. M. R. K.; Möhler, O.; Schnaiter, M.; Wagner, R.; Benz, S.; Niemand, M.; Saathoff, H.; Ebert, V.; Wagner, S.; Kärcher, B. Heterogeneous Nucleation of Ice Particles on Glassy Aerosols under Cirrus Conditions. *Nat. Geosci.* **2010**, *3* (4), 233–237. https://doi.org/10.1038/ngeo817.

(131) Schill, G. P.; Tolbert, M. A. Heterogeneous Ice Nucleation on Phase-Separated Organic-Sulfate Particles: Effect of Liquid vs. Glassy Coatings. *Atmospheric Chem. Phys.* **2013**, *13* (9), 4681–4695. https://doi.org/10.5194/acp-13-4681-2013.

(132) Ignatius, K.; Kristensen, T. B.; Järvinen, E.; Nichman, L.; Fuchs, C.; Gordon, H.; Herenz, P.; Hoyle, C. R.; Duplissy, J.; Garimella, S.; Dias, A.; Frege, C.; Höppel, N.; Tröstl, J.; Wagner, R.; Yan, C.; Amorim, A.; Baltensperger, U.; Curtius, J.; Donahue, N. M.; Gallagher, M. W.; Kirkby, J.; Kulmala, M.; Möhler, O.; Saathoff, H.; Schnaiter, M.; Tomé, A.; Virtanen, A.; Worsnop, D.; Stratmann, F. Heterogeneous Ice Nucleation of Viscous Secondary Organic Aerosol Produced from Ozonolysis of α-Pinene. *Atmospheric Chem. Phys.* **2016**, *16* (10), 6495–6509. https://doi.org/10.5194/acp-16-6495-2016.

(133) James, A. D.; Brooke, J. S. A.; Mangan, T. P.; Whale, T. F.; Plane, J. M. C.; Murray, B. J. Nucleation of Nitric Acid Hydrates in Polar Stratospheric Clouds by Meteoric Material. *Atmospheric Chem. Phys.* **2018**, *18* (7), 4519–4531. https://doi.org/10.5194/acp-18-4519-2018.

(134) Ruzmaikin, A.; Aumann, H. H.; Manning, E. M. Relative Humidity in the Troposphere with AIRS. *J. Atmospheric Sci.* **2014**, *71* (7), 2516–2533. https://doi.org/10.1175/JAS-D-13-0363.1.

(135) Barry, K. R.; Hill, T. C. J.; Levin, E. J. T.; Twohy, C. H.; Moore, K. A.; Weller, Z. D.; Toohey, D. W.; Reeves, M.; Campos, T.; Geiss, R.; Schill, G. P.; Fischer, E. V.; Kreidenweis, S. M.; DeMott, P. J. Observations of Ice Nucleating Particles in the Free Troposphere From Western US Wildfires. *J. Geophys. Res. Atmospheres* **2021**, *126* (3), 1–17. https://doi.org/10.1029/2020JD033752.

(136) Kasparoglu, S.; Perkins, R.; Ziemann, P. J.; DeMott, P. J.; Kreidenweis, S. M.; Finewax, Z.; Deming, B. L.; DeVault, M. P.; Petters, M. D. Experimental Determination of the Relationship Between Organic Aerosol Viscosity and Ice Nucleation at Upper Free Tropospheric Conditions. *J. Geophys. Res. Atmospheres* **2022**, *127* (16), e2021JD036296. https://doi.org/10.1029/2021JD036296.

(137) Altaf, M. B.; Freedman, M. A. Effect of Drying Rate on Aerosol Particle Morphology. *J Phys Chem Lett* **2017**, *8* (15), 3613–3618. https://doi.org/10.1021/acs.jpclett.7b01327.

(138) Petters, M.; Kasparoglu, S. Predicting the Influence of Particle Size on the Glass Transition Temperature and Viscosity of Secondary Organic Material. *Sci. Rep.* **2020**, *10* (1). https://doi.org/10.1038/s41598-020-71490-0.

https://doi.org/10.26434/chemrxiv-2024-5p8pn-v2 **ORCID:** https://orcid.org/0000-0002-5621-2323 Content not peer-reviewed by ChemRxiv. **License:** CC BY 4.0

(139) Shi, S.; Cheng, T.; Gu, X.; Guo, H.; Wu, Y.; Wang, Y. Biomass Burning Aerosol Characteristics for Different Vegetation Types in Different Aging Periods. *Environ. Int.* **2019**, *126* (October 2018), 504–511. https://doi.org/10.1016/j.envint.2019.02.073.

(140) Yu, X.; Shi, C.; Ma, J.; Zhu, B.; Li, M.; Wang, J.; Yang, S.; Kang, N. Aerosol Optical Properties during Firework, Biomass Burning and Dust Episodes in Beijing. *Atmos. Environ.* **2013**, *81*, 475–484. https://doi.org/10.1016/j.atmosenv.2013.08.067.

(141) Ogunjobi, K. O.; He, Z.; Kim, K. W.; Kim, Y. J. Aerosol Optical Depth during Episodes of Asian Dust Storms and Biomass Burning at Kwangju, South Korea. *Atmos. Environ.* **2004**, *38* (9), 1313–1323. https://doi.org/10.1016/j.atmosenv.2003.11.031.

For Table of Contents Only

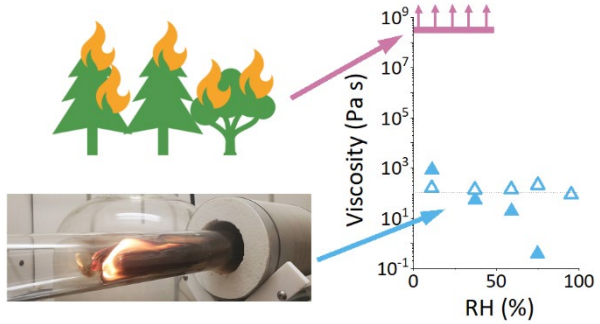

https://doi.org/10.26434/chemrxiv-2024-5p8pn-v2 **ORCID:** https://orcid.org/0000-0002-5621-2323 Content not peer-reviewed by ChemRxiv. **License:** CC BY 4.0